

Crustal structure of Baffin Bay from constrained 3-D gravity inversion and deformable plate tectonic models

J. Kim Welford^{1,*}, Alexander L. Peace¹, Meixia Geng^{1,2}, Sonya A. Dehler³ and Kate Dickie³

¹ *Department of Earth Sciences, Memorial University of Newfoundland, St. John's, NL, Canada*

² *Institute of Geophysics and Geomatics, China University of Geosciences, Wuhan, China*

³ *Natural Resources Canada, Geological Survey of Canada, Dartmouth, NS, Canada*

SUMMARY

Mesozoic to Cenozoic continental rifting, breakup, and spreading between North America and Greenland led to the opening, from south to north, of the Labrador Sea and eventually Baffin Bay between Baffin Island, northeast Canada, and northwest Greenland. Baffin Bay lies at the northern limit of this extinct rift, transform, and spreading system and remains largely underexplored. With the sparsity of existing crustal-scale geophysical investigations of Baffin Bay, regional potential field methods and quantitative deformation assessments based on plate reconstructions provide two means of examining Baffin Bay at the regional scale and drawing conclusions about its crustal structure, its rifting history, and the role of pre-existing structures in its evolution. Despite the identification of extinct spreading axes and fracture zones based on gravity data, insights into the nature and structure of the underlying crust have only been gleaned from limited deep seismic experiments, mostly concentrated in the north and east where the continental shelf is shallower and wider. Baffin Bay is partially underlain by oceanic crust with zones of variable width of extended continental crust along its margins. 3-D gravity inversions, constrained by bathymetric and depth to basement constraints, have

generated a range of 3-D crustal density models that collectively reveal an asymmetric distribution of extended continental crust, approximately 25-30 km thick, along the margins of Baffin Bay, with a wider zone on the Greenland margin. A zone of 5 to 13 km thick crust lies at the centre of Baffin Bay, with the thinnest crust (5 km thick) clearly aligning with Eocene spreading centres. The resolved crustal thicknesses are generally in agreement with available seismic constraints, with discrepancies mostly corresponding to zones of higher density lower crust along the Greenland margin and Nares Strait. Deformation modelling from independent plate reconstructions using GPlates of the rifted margins of Baffin Bay was performed to gauge the influence of original crustal thickness and the width of the deformation zone on the crustal thicknesses obtained from the gravity inversions. These results show the best match with the results from the gravity inversions for an original unstretched crustal thickness of 34-36 km, consistent with present-day crustal thicknesses derived from teleseismic studies beyond the likely continentward limits of rifting around the margins of Baffin Bay. The width of the deformation zone has only a minimal influence on the modelled crustal thicknesses if the zone is of sufficient width that edge effects do not interfere with the main modelled domain.

Keywords: Gravity anomalies and Earth structure, North America, Inverse theory, Plate motions, Continental margins: divergent, Crustal structure

1 INTRODUCTION

Baffin Bay, between Baffin Island, northeastern Canada, and northwest Greenland, is a long and narrow (1350 km by 640 km) ocean basin that lies to the north of the Labrador Sea and Davis Strait (Fig. 1). Due to its remote location and challenging climate, the region has been less explored and studied than more southerly regions in Canada and Greenland. In terms of bathymetry, Baffin Bay (Fig. 2) is shallower (generally < 800 m water depth) than the Labrador Sea to the south (> 3000 m water depth). While the tectonic evolution of Baffin Bay is known to be related to that of the Labrador Sea and Davis Strait, far fewer geophysical investigations have been undertaken in Baffin Bay. Nonetheless, it is clear that Baffin Bay experienced polyphase evolution that included continental rifting, development of transitional crust of indeterminate nature, seafloor spreading (multiple episodes), and periods of intense magmatism (Barrett et al., 1971; Keen & Barrett, 1972;

Keen et al., 1972a; Jackson et al., 1979; Balkwill et al., 1990; Reid & Jackson, 1997; Geoffroy, 2001; Geoffroy et al., 2001; Skaarup et al., 2006; Wilson et al., 2006; Funck et al., 2012; Suckro et al., 2012; Hosseinpour et al., 2013; Suckro et al., 2013; McGregor et al., 2014; Peace et al., 2017). The extended continental shelves on either side of Baffin Bay appear asymmetric with a wider shelf (160 to 200 km) on the Greenland side compared to the Canadian side (40 to 60 km). This seabed asymmetry may be indicative of asymmetry at deeper crustal levels, a characteristic commonly observed at other rifted margins (Chian et al., 1995a; Chian et al., 1995b; Louden & Chian, 1999; Huisman & Beaumont, 2002; Welford & Hall, 2013; Brune et al., 2014; Peace et al., 2016), providing an additional target for geophysical investigation.

Baffin Bay's relatively limited history of oceanic crust production and confined spatial extent make it an excellent target for studying rift tectonics and the emplacement of oceanic crust. These assets, coupled with evidence of extensive magmatism, of debatable origin and asymmetric distribution between margins, allow for multiple tectonic processes to be investigated simultaneously. With the sparsity of existing crustal-scale geophysical investigations of Baffin Bay, regional potential field methods and quantitative deformation assessments based on plate reconstructions provide two means of examining Baffin Bay at the regional scale and drawing conclusions about its crustal structure, its rifting history, and the role of pre-existing structures in its evolution.

2 TECTONIC EVOLUTION

An overview of the geology of Baffin Bay has been produced by Balkwill et al. (1990) and only the most salient points are repeated here. Precambrian crystalline rocks make up the onshore bedrock geology on the flanks of Baffin Bay (Keen et al., 1972b; Balkwill et al., 1990; Jackson et al., 1992; St-Onge et al., 2009; Grocott & McCaffrey, 2017), with instances of non-Precambrian rocks such as flood basalts (Storey et al., 1998; Tegner et al., 1998; Riisager & Abrahamsen, 1999; Geoffroy et al., 2001; Larsen et al., 2009). These continental crustal rocks extend offshore beneath sedimentary basins containing Mesozoic and Cenozoic deposits (Balkwill, 1987). Baffin Bay began rifting, possibly during the Cretaceous, in response to the northward propagation of continental

stretching and rifting in the Labrador Sea and Davis Strait where rifting has occurred since at least the Cretaceous, possibly earlier (Gregersen et al., 2013).

Oceanic crust has been resolved beneath central Baffin Bay (Barrett et al., 1971; Keen & Barrett, 1972; Keen et al., 1972a; Keen et al., 1972b; Jackson et al., 1979; Balkwill et al., 1990; Jackson et al., 1992; Suckro et al., 2012; Funck et al., 2012). While the separation of Greenland from North America was responsible for seafloor spreading in the Labrador Sea starting in the Late Cretaceous (Chron 31 (Keen et al., 2018)), active seafloor spreading in Baffin Bay only began in the Paleocene as Greenland began to simultaneously rift and drift away from Eurasia. This Paleocene seafloor spreading was the first of two episodes of seafloor spreading and has been attributed to the postulated arrival of the ancestral Icelandic mantle plume beneath Greenland (Storey et al., 1998; Gerlings et al., 2009), which is also claimed to have emplaced volcanic sequences on both margins of Baffin Bay as well as significant volcanism to the south in the Davis Strait (Fig. 2). However, more recent work questions this simplistic interpretation, favoring instead the dominance of plate tectonic processes in the tectono-magmatic development of the region (Nielsen et al., 2007; McGregor et al., 2014; Peace et al., 2017).

The opening of the North Atlantic Ocean to the south and to the east of Greenland (Srivastava, 1978) is attributed to have led to the onset of renewed seafloor spreading in Baffin Bay during the Eocene as part of a large-scale reorganisation of North Atlantic tectonics. This new seafloor spreading, which was oriented in a different direction, introduced some transform movement within the Bay affecting the existing Paleocene oceanic crust, resulting in an asymmetric distribution of oceanic crust in the centre of the basin (Oakey & Chalmers, 2012). The renewed seafloor spreading due to the change in plate kinematics contributed to a new pulse of magmatism (Storey et al., 1998), emplacing several hundred metres of volcanic rocks off western Greenland (Nelson et al., 2015). Once seafloor spreading ceased in the Labrador Sea and Baffin Bay at Chron 13, Greenland began to move with North America (Srivastava, 1978).

The sedimentary wedge in Baffin Bay shows a northward thickening from 2 km near Davis Strait to over 14 km in northern Baffin Bay and consists of a combination of both syn-rift and post-rift successions (Balkwill et al., 1990; Gregersen et al., 2013). The syn-rift sedimentary rocks

that fill extensional half-grabens in Baffin Bay are dominantly of Cretaceous age while the post-rift sedimentary rocks filling broader sag basins are dominantly Cenozoic (Gregersen et al., 2013). Seismic reflection interpretation along the northern margins of Baffin Bay reveals evidence for compressional tectonics (Jackson et al., 1992; Whittaker et al., 1997), likely due to contemporaneous compression resulting from the Eurekan Orogeny to the north in the Arctic Islands from Chron 24 to Chron 13 (Balkwill, 1987; Whittaker et al., 1997; Tegner et al., 2011; Stephenson et al., 2013; Heron et al., 2015; Gion et al., 2017; Schiffer et al., 2017).

3 PREVIOUS CRUSTAL STRUCTURE WORK

Wide-angle seismic reflection/refraction profiling techniques, which provide invaluable constraints on velocity structure, depth to Moho, and crustal thickness, have been undertaken across central Baffin Bay since the 1970s (see Fig. 3 for line locations). These experiments have revealed a 4-6 km thick sedimentary package overlying 6-9 km thick oceanic crust (Barrett et al., 1971; Funck et al., 2012; Suckro et al., 2012). Towards Davis Strait to the south, oceanic crust transitions through a 20 km thickened igneous crust to thicker continental crust across the leaky transform Ungava Fault Zone (Funck et al., 2012). Based on the thickened igneous crust transition zone and a high velocity lower crustal layer modelled at the base of the Greenland continental crust toward Davis Strait, Funck et al. (2012) interpreted central to southern Baffin Bay as a volcanic/magma-rich set of rifted continental margins.

Seismic refraction profiling along the Greenland margin in northeastern Baffin Bay has revealed anomalously thin oceanic crust (3.5 to 7 km thick) toward the centre of Baffin Bay, separated from continental crust to the northeast by a 60 km-wide interpreted magmatic feature (Altenbernd et al., 2014; Altenbernd et al., 2015). The thin oceanic crust is modelled as being underlain by partially serpentinized mantle and is interpreted as resulting from ultraslow seafloor spreading with a limited magma supply.

At the northwestern limit of Baffin Bay, older seismic refraction work (Reid & Jackson, 1997) revealed a continent-ocean transition zone which was underlain by serpentinized mantle, similar to the transition zones generally associated with non-volcanic/magma-poor margins, which has

been confirmed by more recent studies (Altenbernd et al., 2016). As pointed out by Funck et al. (2012), these conflicting results compared to central and southern Baffin Bay imply that a non-volcanic/magma-poor to volcanic/magma-rich transition occurs somewhere between central and northern Baffin Bay, similar to the transition interpreted for the Labrador Sea further south (Keen et al., 2012).

Onshore, along the margins of Baffin Bay and Greenland, no controlled-source seismic surveys have been acquired. However, there have been efforts to estimate Moho depth and crustal thickness using passive seismic methods such as receiver function modelling (Dahl-Jensen et al., 2003; Darbyshire, 2003). These reveal that for the Archean cratons making up northern and central Baffin Bay, present-day crustal thicknesses are on the order of 34 km for Ellesmere Island, 35 km for northern Baffin Island, and 35-40 km along the Greenland margin (Dahl-Jensen et al., 2003). Further south, the crust thickens to 39-46 km in the Proterozoic orogenic belts beneath southern Baffin Island (Darbyshire, 2003).

At the broader scale of the Labrador Sea and Baffin Bay combined and of the Arctic region, gravity inversion and plate reconstruction studies (Alvey et al., 2008; Hosseinpour et al., 2013) have been used to derive crustal thicknesses and stretching factors. While Baffin Bay was included in the Alvey et al. (2008) study, the results for Baffin Bay were not discussed in detail and the scale of the resulting maps make it difficult to extract regional structures from within the bay. From the more recent Hosseinpour et al. (2013) study, the crust at the centre of Baffin Bay is on the order of 5 to 9 km thick with up to an additional 8 km of igneous crust emplaced along the leaky Ungava Fault Zone. Along the margins of Baffin Bay, the thickness of crust beneath the continental shelves is between 22 and 32 km.

4 GRAVITY INVERSION

Satellite free air gravity data (Fig. 3A) were obtained for Baffin Bay from the DNSC08 compilation from the National Space Institute of the Technical University of Denmark (Andersen et al., 2010). These data are freely available and are an updated and augmented version of an earlier compilation of satellite altimetry data from Sandwell & Smith (1997) of the results from both the

Geosat Geodetic Mission and the ERS 1 Geodetic Phase mission. The data reveal highly variable gravity anomalies in Baffin Bay (Fig. 3). Gravity lows are observed around the margins of the bay, particularly over Melville Bay, which is a major depocentre with at least 7 km of sedimentary rocks (Keen & Barrett, 1972; Whittaker et al., 1997). Gravity highs are mostly concentrated in the north and on the Greenland side of Baffin Bay. These highs are discontinuous and do not reveal any interpretable patterns. To the south in the Davis Strait, the distribution of gravity anomalies appears more symmetric (Fig. 3).

4.1 Methodology

Regional depth to Moho and crustal thickness estimates are commonly derived using 3-D gravity inversion techniques (Welford & Hall, 2007; Kimbell et al., 2010; Welford et al., 2010; Cowie & Kusznir, 2012; Hosseinpour et al., 2013; Welford & Hall, 2013), particularly in regions with limited deep seismic coverage. For Baffin Bay, we are applying the same methodology applied to earlier work on the Newfoundland (Welford & Hall, 2007; Welford et al., 2012), Irish Atlantic (Welford et al., 2010), Labrador Sea (Welford & Hall, 2013), and Nova Scotian (Dehler & Welford, 2013) margins. For all of these previous studies, the GRAV3D inversion algorithm (Li and Oldenburg (1996; 1998)) has provided interpretable crustal-scale results using only bathymetric and depth to basement constraints. To assess the non-uniqueness of the GRAV3D inversion results, we also compare the GRAV3D results with results from a newly developed 3-D constrained gravity inversion method (Geng et al., submitted; Geng et al., 2017), based on the probabilistic method (Chasseriau & Chouteau, 2003; Tarantola, 2005), that more easily allows for the incorporation of additional sparse constraints such as Moho depth.

Briefly, the gravity inversion algorithms used for this study take gravity observations acquired at the surface of the Earth and produce a subsurface 3-D model of density anomalies. These anomalies are specified relative to a prescribed reference density. For the GRAV3D algorithm, previous experience has informed the interplay between choice of model mesh depth and choice of reference density that provides the best correspondance between the inverted Earth model and available deep seismic constraints (Welford & Hall, 2007; Welford et al., 2010; Welford et al., 2012; Dehler

& Welford, 2013; Welford & Hall, 2013). The inversion results can be further tailored by the use of bathymetric and depth to basement constraints to keep certain portions of the model invariant (e.g., seawater), or other portions only moderately variant (e.g., sedimentary column). By prescribing the density structure of the shallow part of the model, which is best constrained, the inversion is permitted to smoothly distribute remaining mass anomalies, required to fit the observations, throughout the deeper or less constrained portions of the model, using a prescribed depth-weighting function. The inversion process involves a tradeoff between minimizing a data misfit (how well the observations are reproduced) and satisfying a model norm (the type of model desired, i.e., smooth or blocky).

GRAV3D uses a parameterization of rectangular prisms that can each be of arbitrary size and that are each assigned a constant density anomaly value. For large regional, crustal-scale applications, we use laterally broad prisms (5 km by 5 km) with a limited depth extent (500 m). For the study region shown in Figure 2, these parameters produce a model with 230 cells in the eastings direction, 300 cells in the northings direction, and 80 cells in depth for a total model depth of 40 km. A similar study in the Labrador Sea showed that the best match with available seismic constraints was achieved with these model dimensions and a reference density of 2950 kg/m³ (Welford & Hall, 2013).

The new constrained probabilistic inversion method (Geng et al., submitted; Geng et al., 2017), used for comparison with the GRAV3D results, involves a different methodology but a similar parameterization. The new method controls model smoothness by using a model covariance matrix, and linear equality constraints allow boundary constraints to be incorporated directly into the inversion. In contrast to GRAV3D, this method foregoes the use of a depth weighting function by incorporating constraints on allowable average layer densities as a function of depth. This approach results in inverted models that can more easily incorporate density jumps without imposing them as hard boundaries in the model. The constrained probabilistic inversion method was tested on a subset of the regional data (outlined by the dashed black rectangle in Fig. 1) using a coarser parameterization of 10 km by 10 km by 1 km in depth due to computational limitations.

4.2 Use of Data Constraints

Bathymetric constraints are readily available. For this study, the 2014 global 30-arcsec gridded bathymetric data set (http://www.gebco.net/data_and_products/gridded_bathymetry_data) of the General Bathymetric Chart of the Oceans (GEBCO) was used (Fig. 4A). In the reference density anomaly model used for the inversions, prisms between the top of the model and the bathymetry were assigned the density of seawater (relative to the reference density) and were not allowed to vary during the inversion.

Only spatially-limited depth to basement constraints are available for Baffin Bay as the existing depth to basement database of the Geological Survey of Canada does not extend into Baffin Bay (Oakey & Stark, 1995; Loudon et al., 2004) and the sediment thickness estimates from the National Geophysical Data Centre (NGDC) of the National Oceanic and Atmospheric Administration (NOAA) Satellite Information Service (Divins (2003); <http://www.ngdc.noaa.gov/mgg/sedthick/>) only extend partway into Baffin Bay (outlined by thick purple dashed line in Fig. 4B). While depth to basement contours are presented by Balkwill et al. (1990), the source of those constraints is not provided. Consequently, depth to basement was interpreted along legacy industry seismic profiles over the region outlined in the thick dotted black line in Figure 4B. Since the interpretation was performed on two-way traveltimes data, the basement picks were converted to depth using a time to depth relationship derived using well logs from the Labrador Sea to the south (C. Keen, personal communication). For remaining parts of Baffin Bay where industry and NOAA depth to basement estimates were unavailable, depth to basement was digitized from sparse seismic refraction models. The depth to basement map shown in Figure 4B was obtained by smoothly interpolating through all of the available depth to basement constraints, without accounting for absolute uncertainties in individual depth to basement values. These uncertainties are ultimately obscured by the blocky inversion parameterizations.

For the inversions, prisms corresponding to sedimentary rocks between the bathymetry and the basement within the reference density anomaly model were assigned depth-dependent densities consistent with sedimentary lithologies (Fig. 5). These density anomalies were only allowed to vary between geologically reasonable depth-dependent density bounds for sedimentary rocks (Fig.

5). It is important to note that the deepest section of sedimentary rocks in the north of Baffin Bay is constrained by just three seismic refraction models (A14, Altenbernd et al. (2014); A16, Altenbernd et al. (2016); R4, Reid and Jackson (1997)), with the deepest constraints coming from the oldest survey (Reid & Jackson, 1997). Thick sequences of sedimentary rock were previously inferred for northern Baffin Bay (Keen & Barrett, 1972; Keen et al., 1972b). The presence of very deep sedimentary basins in northern Baffin Bay does not adversely affect the inversion results since the deepest sediments have density anomalies that approach those of basement rock (Fig. 5).

Below the prescribed seawater and sedimentary layers in the reference density anomaly models, the inversions were given greater freedom (i.e., broader bounds) to vary density anomalies within the model in order to reproduce the observed free air gravity anomalies. In total, three separate inversions were run and each was able to generate a regional 3-D density anomaly model for Baffin Bay, down to 40 km depth, that respected all available constraints and were consistent with the observations, within 10 mGal for most of the study region (Fig. 3B).

For the first inversion, the GRAV3D algorithm was used with only bathymetric and depth to basement constraints. Seawater density was kept invariant and density anomalies (and their acceptable bounds) within the sedimentary basins were assigned according to the constraints from Figure 5. Below the sedimentary basins, all remaining model cells were assigned the same starting density anomaly value and the same broad range of acceptable density anomalies.

For the second inversion, the GRAV3D algorithm was used again with the same shallow constraints as before, but this time with one additional model boundary, corresponding to the base of the crust (i.e., the Moho). This layer boundary was obtained by smoothly interpolating through the available depth to seismic Moho constraints (Fig. 6C) and was inserted into the reference density anomaly model with an abrupt density contrast across the sparsely-constrained boundary. By incorporating the Moho as a laterally continuous model boundary, the inversion was forced to fit the gravity observations by altering the density anomalies within the crust and mantle, respectively, without altering the geometry of the Moho boundary.

The third and final inversion involved the use of the new probabilistic inversion method (Geng et al., submitted; Geng et al., 2017) and incorporated the sparse Moho constraints directly into

the inversion as localized density gradient point pairs with a contrast of 485 kg/m^3 , the estimated global average for the density contrast across the Moho boundary (Tenzer et al., 2012). The sparse Moho constraints were assigned a large standard deviation error of 150 kg/m^3 to account for errors caused by the variable quality and vintage of the seismic constraints.

The goal of performing three separate inversions using different methodologies but similar constraints was to better understand the non-uniqueness of the inverted results and to extract common features from the models for interpretation. The models are assessed and compared in the following sections.

4.3 Results: Depth to Moho and Crustal Thickness

For the resolved 3-D density anomaly models for Baffin Bay, the base of the crust was approximated by defining a density anomaly isosurface that represents a Moho proxy. For the reference density chosen, the base of the crust/Moho proxy isosurface was defined as 70 kg/m^3 (corresponding to an absolute density of 3020 kg/m^3), as this value showed the best correspondence with most of the available deep seismic constraints. The resulting depth to the Moho proxy from the first inversion is plotted in Figure 6A. Generally, the margins of Baffin Bay correspond to a Moho depth of approximately 25 to 30 km while the west-central part corresponds to an average Moho depth of approximately 15 km. A Moho depth of approximately 25 km is observed to the north in Nares Strait and to the south through Davis Strait.

By simply interpolating between depth to Moho constraints from the sparse seismic refraction modelling, a uniformly shallower Moho is obtained through central Baffin Bay while the crust offshore Greenland appears significantly thicker, based largely on contributions to the interpolation from teleseismic Moho estimates onshore (Dahl-Jensen et al., 2003; Darbyshire, 2003). For the Baffin Island margin, very few seismic constraints are available and a smooth variation in Moho depth is interpolated between the teleseismic Moho constraints from the centre of the island to the seismic refraction results through oceanic crust in southern Baffin Bay. In contrast, the Moho proxy from the gravity inversion (Fig. 6A) shows a more abrupt crustal necking offshore Baffin Island. The interpolation results through Nares Strait are highly variable due to the coincident seismic

refraction results showing differing Moho depths and the onshore teleseismic Moho constraint being very deep (chosen as 37 km in the interpolation based on the estimate of 35 to 40 km from Darbyshire (2003)). These complicate the interpolation and result in a highly variable Moho immediately offshore.

By combining the Moho proxy depth from the first inversion with the interpolated depth to basement map (Fig. 4B), an estimate of crustal thickness across Baffin Bay can be made based on the gravity inversion results (Fig. 6B). This map reveals crustal thicknesses between 25 to 30 km for most of the margins of Baffin Bay while the central part is generally 10 km thick. Of note, two WNW-ESE oriented corridors of thinner crust (approximately 5 km thick) are observed in the north, aligned with Lancaster Sound, and in the south, roughly aligned with seismic line F12. Thinner crust is also observed beneath the Melville Basin and in Lancaster Sound, as has been previously noted by Oakey & Chalmers (2012). The crust in Davis Strait is on the order of 20 km thick, as has been previously documented (Keen & Barrett, 1972; Funck et al., 2012).

For comparison, the same crustal thickness calculation was performed using the interpolated seismic Moho (Fig. 6C) with the result plotted in Figure 6D. As with the observations for the interpolated seismic Moho, similar patterns arise. Central Baffin Bay appears to be underlain by a broader region of highly thinned crust (less than 5 km thick) while the margins of the basin have thicknesses on the order of 25 km.

4.4 Results: Profile Comparisons

By slicing the resolved 3-D density anomaly models along existing seismic refraction lines, a direct comparison can be made between the inferred Moho proxy and depth to Moho obtained from seismic refraction modelling. Slices for all available deep seismic lines are shown for the first and second inversions using GRAV3D in Figures 7 and 8, respectively. In Figure 9, select slices from all three inversion approaches are compared.

Generally, the slices through the model with only bathymetric and depth to basement constraints (Fig. 7) show a good match between the Moho proxy and the seismic Moho, with an error of less than 5 km, making the Moho proxy a good first order estimate of the base of the crust

beneath Baffin Bay. Comparing these slices with those obtained from the second inversion where the seismic Moho was prescribed as a sharp and continuous boundary (Fig. 8) can help differentiate between mismatches due to poor/conflicting seismic constraints or due to anomalous crustal features.

Nares Strait at the northern limit of Baffin Bay provides the largest mismatch between the Moho proxy and the seismic Moho along profile R3 (Fig. 7). This older seismic refraction profile is almost coincident with the more recent profile, A16, where a similar mismatch toward the NNW is observed. The observed gravity along profile R3 is relatively constant, in contrast to the large change in the seismic Moho depth modelled by Reid & Jackson (1997) which would be expected to be accompanied by a pronounced gravity gradient. The longer profile for A16 does capture a gravity anomaly decrease toward the NNW but the resolved crustal thickening required by the inversion to reproduce that observation is not as extreme as the one captured by the seismic refraction modelling (Altenbernd et al., 2016). For both of these profiles, the second inversion with the prescribed Moho boundary (Fig. 8) shows that a relatively higher density lower crust is required northward beneath Nares Strait in order to satisfy both the seismic and the gravity constraints. Note that the mismatches between the regionally interpolated seismic Moho and the plotted seismic Moho along profiles R3 and A16 in Figure 8 result from conflicting Moho depths from different surveys all being included in the interpolation. These mismatches aren't surprising given the complexity of the Nares Strait region where narrow localized basins have been imaged and a dormant transform fault, possibly reactivated by compression during the Eurekan Orogeny, has been interpreted (Keen et al., 1972a; Reid & Jackson, 1997).

More minor mismatches between the seismic Moho and the Moho proxy are observed toward the Greenland margin on profiles S12, F12, and A15 (Fig. 7). The crustal density distributions along all of these profiles can be made to match the seismic Moho by incorporating pockets of higher density material into the lower crust (Fig. 8). The need for these higher density lower crustal zones appears to diminish to the north along profile A14. The Moho-proxy from the third probabilistic inversion does a better job of reproducing the seismically-resolved Moho structure but there is still a discrepancy where higher density lower crustal material is required (Fig. 9C).

It is impossible to test whether similar higher density lower crustal pockets are required on the Baffin Island margin due to the lack of deep seismic constraints.

At the northwestern end of profile F12 in Figures 7, 8, and 9, there is significant disagreement between the results from the three inversion approaches. For the second inversion (Figs. 8 and 9B), the smooth interpolation between the limit of the refraction constraints (thick black line) and the teleseismic Moho depth constraint in the middle of Baffin Island results in the gradual deepening of the Moho from 14 to 17 km between model distances of 0 to 70 km. This region corresponds to a localized gravity low where the second inversion is forced to place very low densities in the crust in order to respect the interpolated seismic Moho. A similar but less extreme upper crustal lowering of density is obtained using the probabilistic inversion method where sparse Moho constraints were used (Fig. 9C). In contrast, the gravity inversion results obtained with only bathymetry and basement constraints (Fig. 7) produce a more abrupt deepening of the Moho down to 25 km at this location along F12. The resulting crustal density structure in Figure 7 provides a more geologically reasonable crustal structure in this region where no other deep seismic constraints are available, as compared to the other two inverted models. This suggests that the inclusion of sparse Moho constraints in the inversion can adversely skew the resolved models if the region of interest shows significant lateral variability in density structure and the inversion is tasked with generating a laterally smooth model.

4.5 Results: Oblique Slices

Arbitrary oblique slices were extracted from the density anomaly models obtained from the first and third inversions (Fig. 10) in order to visualize the variations in crustal thickness at regular intervals along strike within Baffin Bay. The results from the second inversion were not included in this comparison as the reliability of the interpolated Moho surface diminishes away from the seismic lines from which the constraints were obtained, and the resulting density anomaly structures are less well constrained. The co-located slices in Figure 10 show many similar trends but also several discrepancies, mostly due to the coarser parameterization used for the probabilistic inversion, enhanced by a higher degree of lateral smoothing applied in that method.

Slice A-A' in northern Baffin Bay shows a distinct asymmetry with thicker crust on the Greenland margin and a wide zone of thinner crust in the centre of the basin. The Moho trends obtained from the two inversion methods are similar although the slice from the first inversion shows greater lateral variability in crustal thickness. Along the Greenland margin, landward of the Melville Basin, this variability is equivalently modelled by the probabilistic inversion method using higher upper crustal densities. The difference map computed from the two crustal thickness estimates (Fig. 10C) shows that the first inversion produced a crust that was 8 km thinner, immediately landward of the Melville Basin. Seismic refraction line A14 (Altenbernd et al., 2014) coincides with slice A-A' and shows a shallowing of the Moho at this location of only 3 km (Fig. 7) and typical upper crustal densities, while the probabilistic inversion failed to capture the Moho variability due to the high standard deviation error assigned to the sparse seismic Moho constraints. Based on the results presented in Figure 10, the density structure along slice A-A' would appear to correspond to a hybrid model between the two inverted model slices.

Further south, slice B-B' passes through a zone of anomalously thin crust (Fig. 10A) that appears to coincide with the southeastward limit of the Eocene spreading centre. The model from the GRAV3D inversion shows an abrupt necking of the crust at this location while the probabilistic inversion maintains a deeper Moho while imposing higher densities in the overlying crust in order to satisfy the observed gravity response. At the Greenland end of the profile, the GRAV3D inversion results show another thinning of the crust while the probabilistic inversion satisfies the gravity observations by placing higher densities within the upper crust. Again, based on the coincident seismic refraction line A15 (Altenbernd et al., 2015), the true density structure appears to lie somewhere between the two inverted model slices as the seismic Moho does exhibit significant lateral variability (Figs. 7 and 9) while the upper crustal densities are not anomalously high (Altenbernd et al., 2015).

Profile C-C' in central Baffin Bay shows a good correspondence between the crustal structure derived from the two inversion methodologies although the GRAV3D inversion generates a thicker crust toward Baffin Island where no seismic constraints are available. The difference map computed from the two crustal thickness estimates (Fig. 10C) shows that the GRAV3D inversion adds

an extra 4-8 km of crust to the Baffin Island margin. As shown in Figure 9, this addition of crust prevents the inversion from requiring anomalously low densities in the upper crust (as is produced by the other inversions) and arguably provides a more geologically reasonable cross-section. These results suggest that the incorporation of Moho constraints may not always lead to better results, particularly when the crust is laterally variable in thickness and composition.

The oblique profile D-D' in southern Baffin Bay shows an excellent match in crustal structure using the two methods, with only a slight shift in overall Moho depth. Again, the GRAV3D results appear to resolve the localized thinning of the crust associated with the ancient seafloor spreading axis while the probabilistic inversion generated a smoother cross-section. The difference map computed from the two crustal thickness estimates (Fig. 10C) confirms that the crustal thickness estimates are within a few kilometers of each other.

5 MODELLING CRUSTAL THICKNESS USING GPLATES

The GPLates tectonic modelling and visualisation software package (Boyden et al., 2011; Williams et al., 2012; Cannon et al., 2014) has been used for a wide array of geological and geophysical applications (e.g., Gibbons et al. (2012), Phethean et al. (2016)). One such application of GPLates is to model crustal thickness through time based on either an implied initial uniform crustal thickness or through the calculation of a crustal thinning factor within a defined deformable zone (e.g., Gurnis et al. (2018), and Müller et al. (2018)). Irrespective of other crustal thickness estimates, GPLates models of crustal thickness can provide useful insights into the geodynamic evolution of a region including the timing and extent of thinning. However, in conjunction with crustal thickness estimates derived using independent methodologies, such as the constrained gravity inversions presented herein, insights can be made into: 1) the reliability of crustal thickness estimates derived using other such methods, 2) the original, pre-rift crustal thickness, 3) the spatial-temporal evolution of crustal thinning, and 4) the reliability of the model inputs such as the poles of rotation and continent-ocean boundaries (COBs).

5.1 Methodology

The model described herein was built in GPlates 2.0.0 using the global poles of rotation compilation of Matthews et al. (2016), which for Baffin Bay and the Labrador Sea uses the poles of rotation from Lawver et al. (1990) and Barnett-Moore et al. (2016). The methodology and theory behind GPlates deformable plate models such as those deployed herein are described in detail in Gurnis et al. (2018).

Three different deformable zones were defined. These extend continent-ward from the continent-ocean boundary (COB) proposed by Hosseinpour et al. (2013), have variable rift zone half-widths of 150 km, 300 km, and 450 km, and are similar to the various unstretched continental crust boundaries of Hosseinpour et al. (2013). The broad range of variable widths to test were chosen as onshore, rift-related deformation has been shown to extend several hundred kilometres from the COB in the area (Hosseinpour et al., 2013; Peace, 2016). All modelled deformation occurs within this deformable zone of continental crust and is produced by absolute plate motions resulting in strain accumulation which can be modelled as the change in crustal thickness over time as:

$$dH/dt = -H \times S \quad (1)$$

where H corresponds to crustal thickness, S is the strain dilatation rate, and t is time (Gurnis et al., 2018). For all the models presented in this study, uniform crustal thicknesses of 34, 36, 38, and 40 km were assumed for 200 Ma, prior to the onset of significant continental rifting (Larsen et al., 2009; Abdelmalak et al., 2012).

The age and locations of the COBs in the Labrador Sea, Davis Strait, and Baffin Bay are taken from the global compilation of Müller et al. (2016), which for Baffin Bay uses those of Hosseinpour et al. (2013) based on the interpretation of seismic reflection profiles and potential field data. In the Müller et al. (2016) compilation, breakup is considered to occur at 90 Ma in the southern Labrador Sea, 70 Ma in the northern Labrador Sea and Davis Strait, whilst in Baffin Bay breakup is said to occur at 63-64 Ma. These ages conflict with recent work by Keen et al. (2018) who argue for breakup at 70 Ma in the central Labrador Sea, and work from Oakey & Chalmers (2012) who argue for breakup in Baffin Bay at Chron 27 (62 Ma).

For this study, we assume COB appearance to be simultaneous and synonymous with breakup based on the global Müller et al. (2016) model. However, in the original Hosseinpour et al. (2013) model, true oceanic crust is said to occur after 61 Ma (i.e., a longer period of continental rifting than in the Labrador Sea). Furthermore, Hosseinpour et al. (2013) include oceanic crust in the Davis Strait where previous work suggests crust of predominantly continental affinity (Funck et al., 2007; Suckro et al., 2013). Despite these potential timing and crustal affinity issues with the Hosseinpour et al. (2013) model, it is used herein to provide a first-order estimate of crustal thickness through time as redefining these model inputs to address the issues outlined is far beyond the scope of this study. Finally, the external topological boundaries from Gion et al. (2017) of the Eurekan orogeny, to the north of Baffin Bay, were used as the northern boundary to the deformable zone in our model as this orogeny was cotemporaneous with a change in extension direction and was also modelled in GPLates by Gion et al. (2017).

5.2 Results

Results of the GPLates modelling are presented in Figure 11 for a range of initial crustal thicknesses and a range of deformation zone half-widths. These are plotted alongside the crustal thicknesses derived from the constrained 3-D gravity inversion using GRAV3D without Moho constraints (Fig. 11A) and from the interpolated seismic Moho (Fig. 11B).

Figure 11 reveals that the width of the deformable zone has a minimal influence on the final crustal thickness if the zone is of sufficient width that edge effects do not interfere with the main modelled domain. Generally, the 300 km wide zone was found to be beyond the influence of significant edge effects, whilst models of 450 km demonstrate that the results do not vary greatly from those of 300 km. When compared to the crustal thickness estimates derived through the gravity inversion constrained by seismic and bathymetric data (Fig. 11A), the best correspondance is observed for initial crustal thicknesses of 34 to 36 km, for both the east and west margins of Baffin Bay.

Features present on both the gravity inversion and the GPLates models are more likely to result from large-scale tectonics rather than localized manifestations of deformation (e.g., reactivation of

discrete structures). Such features present on both models include an average crustal thickness of approximately 25 km on both margins and a thickening of the crust in Disko Bay (Fig. 11), and in pockets along the margin of Baffin Island, with a localized crustal thickening in both models offshore southeast Baffin Island, which is juxtaposed against a thinner zone offshore southwestern Greenland.

While zones of highly thinned crust (approximately 15 km thick) are resolved in Melville Bay by the GRAV3D gravity inversion, these are not present in the GPLates models. This may demonstrate that although large-scale tectonics control the regional thinning (as displayed in the GPLates model), the small-scale manifestations, as displayed on the gravity inversion results, are controlled by localised factors such as reactivation of discrete structures, a process known to be influential in the area (Doré et al., 1997; Wilson et al., 2006; Peace et al., in press).

Although there is general agreement between the models, the GPLates models estimate significantly thicker crust in northernmost Baffin Bay and Nares strait when compared to the gravity inversion results. This is likely to be due to the poorly constrained tectonics in this region that were input into the GPLates model rather than an error in the gravity inversion. Overall, however, as the GPLates model was broadly able to replicate, to first order, the results of the gravity inversions, the GPLates model inputs (e.g., poles of rotation and COB locations from Hosseinpour et al. (2013), Matthews et al. (2016), Barnett-Moore et al. (2016)) have therefore been independently verified as being reasonable estimates for reconstructions of regional tectonic events, despite the timing and crustal affinity concerns outlined in the previous section.

As described, the closest match between the gravity inversion results and the GPLates modelling is for an initial crustal thickness of 34-36 km with a rift zone half-width of 300 km (Figure 11). The temporal development of the model for 34 km with a rift zone half-width of 300 km is provided in Figure 12 to show the predicted crustal evolution for this model setup over time. Similar evolutions are predicted for the other models (not shown).

First, it can be seen that prior to breakup (as defined by the COBs of Müller et al. (2016) and Hosseinpour et al (2013)), crustal thinning is relatively evenly distributed across the deformable domain. However, as breakup propagates northwards from the Labrador Sea into Baffin Bay, more

localised thinning is observed in the proto-Baffin Bay region while the region to the north retains thicker crust for longer. Post-breakup (65 Ma), variations in the crustal thickness along both the eastern and western margins of Baffin Bay are predicted, with the regions around southern Baffin Island and Disko Bay retaining thicker crust than surrounding regions. The models of the post-breakup interval also predict significant crustal thickening in northern Baffin Bay and in the Arctic region associated with the northward movement of Greenland during the Eurekan orogeny.

6 DISCUSSION

Constrained 3-D gravity inversions have provided regional 3-D density anomaly models for the entirety of Baffin Bay. These models, which complement existing seismic constraints, allow for the delineation of regional trends that can contribute to our knowledge of the tectonic evolution of Baffin Bay.

6.1 Crustal Thickness Variations

Oblique slices through the inverted density anomaly models, derived with and without the incorporation of sparse Moho constraints (Fig. 10), show lateral variations in crustal thickness across Baffin Bay. Based on the density anomaly values alone, it is impossible to distinguish between oceanic and thinned continental crust so we rely on the published literature to define crustal types.

A simplified geological map for Baffin Bay (Fig. 13A) is plotted alongside the map of crustal thickness derived from the GRAV3D gravity inversion using only bathymetric and basement constraints (Fig. 13B), and a crustal thickness difference map computed from the results of the GRAV3D inversion (without Moho constraints) and the probabilistic inversion with sparse Moho constraints (Fig. 13C). The crustal thickness map (Fig. 13B) is further overlain by thickened orange lines that show regions where the GRAV3D inversion with a forced Moho boundary required relatively higher density lower crust in the inverted model in order to satisfy the gravity observations. These high density lower crustal regions exceed the constant density anomaly value used to approximate the base of the crust/Moho proxy for the other two inversions, and so do not appear in the crustal thickness difference map (Fig. 13C). The spatial distribution of these higher density

lower crustal zones approximately corresponds to the spatial extent limits on Paleogene basalts, possibly suggesting a link between the two.

Overall, the thinnest crust in Baffin Bay corresponds to oceanic crust according to Figure 13B, although this thinner crust extends further westward than indicated by the continent-ocean boundary proposed by Hosseinpour et al. (2013). Within this inferred zone of thinner oceanic crust, the most striking feature to stand out from Figure 13B is the alignment of the WNW-ESE corridors of thinnest crust with the extinct Eocene spreading centres (dashed gray lines in Fig. 13) from Oakey & Chalmers (2012), although the northwestern limit of the ridge should perhaps be realigned with Lancaster Sound, a link already proposed by Jackson et al. (1979) and by Oakey & Chalmers (2012).

The degree of lateral variability in crustal thickness across Baffin Bay appears to be linked to the interplay between the orientations of the spreading centres and of the rifted margins. In the north-central part of Baffin Bay where the spreading centre has an oblique orientation relative to the original rifting axis, the crustal structure appears to exhibit a more abrupt necking (Fig. 10, profile B-B'), with thin oceanic crust juxtaposed against thicker continental crust. Further south, where the extinct spreading centre remains closer to the centre of bay, the crustal structure is more laterally smooth with only a more gradual thickening toward Greenland (Fig. 10, profiles C-C' and D-D').

Although the GPlates modelling produces essentially symmetrical thinning of the deformable zone that can be assumed to approximate, large-scale, pure shear deformation, the results allow us to comment on how reasonable the pure shear assumption is and thus indirectly make assertions regarding asymmetric rifting. It should be noted however, that the margins produced in the models are inherently asymmetric due to the implied locations of the COB on each conjugate margin (Hosseinpour et al., 2013). As comparable results were produced from the gravity inversions and the GPlates modelling, it would appear that at the scale of individual margins, pure shear deformation dominates. Due to the inherent GPlates model setup, however, the results are not sufficient to allow us to comment on asymmetry across the conjugate margin pair. Still, given the variable

margin widths (Hosseinpour et al., 2013), it seems plausible that rifting of Baffin Bay was, as with the Labrador Sea (Peace et al., 2016), asymmetric.

6.2 Pre-existing Structures

Most of the onshore margins of Baffin Bay consist of Archean cratonic domains, with Proterozoic orogenic belts dominating in the south (Fig. 2). The location of the transition between these domains remains uncertain, particularly in Greenland where it is obscured by significant ice cover. For this study, the onshore Archean/Proterozoic boundaries from Darbyshire (2003) and St-Onge et al. (2009) are used for Baffin Island and Greenland, respectively. The extrapolation of these boundaries offshore into Baffin Bay does not reveal an obvious correlation between variations in the resolved crustal thicknesses offshore and the different unstretched crustal thicknesses onshore. However, when the difference between the crustal thicknesses derived from the GRAV3D inversion without Moho constraints and those derived from the probabilistic inversion using sparse Moho constraints are computed, an additional 4-8 km of crust is resolved by the GRAV3D inversion immediately offshore Baffin Island (Figs. 10C and 13C). The southern boundary of this thicker crust appears to align with the trend of the onshore suture between the Archean and Proterozoic domains on Baffin Island (Fig. 10C and Fig. 13C). On the Greenland margin, an abrupt crustal thickness difference is observed further south than the proposed transition between Archean and Proterozoic domains from St-Onge et al. (2009). This boundary may not be geologically significant or it may mean that the boundary on the Greenland side is incorrectly located. Unfortunately, both of these regions are lacking deep seismic coverage so a definitive confirmation is not currently possible.

The presence of thicker Proterozoic orogens prior to rifting at the southern end of Baffin Bay does not appear to have strongly impacted subsequent extension and rifting. The results from the deformation modelling using GPlates reveal that the offshore crustal thicknesses derived from the constrained 3-D gravity inversions can be predicted from the independent plate reconstruction by using the onshore crustal thicknesses of the Archean domains from teleseismic studies as representative of the initial unstretched crustal thickness.

7 CONCLUSIONS

Constrained 3-D gravity inversions were used to generate 3-D density anomaly models for Baffin Bay, northeastern Canada/northwest Greenland. The resulting models are all able to reproduce the observed gravity anomalies while showing consistency with available independent seismic constraints. Estimates of Moho depth and crustal thickness were obtained by selecting a density anomaly isosurface as a base of the crust/Moho proxy within the models. Analyses of the resulting maps and slices through the 3-D model have revealed:

- The depth to Moho beneath Baffin Bay varies from 25 km along its margins to 15 km at its centre.
- Crustal thickness varies beneath Baffin Bay with values of 25 to 30 km along its margins, asymmetrically distributed, and 10 km or less in the west-central part of the basin.
- Slices through the density anomaly model generally confirm the crustal structure obtained from coincident deep seismic experiments, with mismatches requiring the inclusion of pockets of relatively higher density lower crust.
- Two WNW-ESE corridors of thinner crust (approximately 5 km thick) align with the extinct Eocene spreading centres, and their orientations, relative to the original rifting orientation, may control the degree of apparent crustal asymmetry.

The explicit incorporation of seismic Moho constraints into the gravity inversions, whether as a continuous surface or as localized constraints, does not always yield the most geologically-reasonable models, as the stricter Moho constraints often result in the inversion placing unreasonable densities in other portions of the model to compensate. Consequently, greater interpretive value can be obtained by running multiple inversions with similar input parameters and different methodologies, in order to better assess the factors contributing to the observed gravity values.

Overall, the complementary GPlates crustal thickness models have shown that to a first order approximation the values produced by the gravity inversions are reasonable and that the pre-rift crustal thickness in the area is likely to have been close to 34-36 km. Furthermore, the main

influence on the final crustal thickness is 1) the initial crustal thickness, 2) the geometry of the conjugate rift flanks, and 3) localized effects such as reactivation.

ACKNOWLEDGMENTS

Support for this study was provided by Natural Resources Canada through the Geo-mapping for Energy and Minerals Program. The Hibernia Project Geophysics Support Fund provided salary support for Alexander L. Peace. The China Scholarship Council provided salary support for Meixia Geng. Natural Resources Canada Contribution No. 20170333.

REFERENCES

- Abdelmalak, M., Geoffroy, L., Angelier, J., Bonin, B., Callot, J., Gélard, J., & Aubourg, C., 2012. Stress fields acting during lithosphere breakup above a melting mantle: a case example in West Greenland, *Tectonophysics*, **581**(doi:10.1016/j.tecto.2011.11.020), 132–143.
- Albertz, M., Beaumont, C., Shimeld, J., Ings, S., & Gradmann, S., 2010. An investigation of salt tectonic structural styles in the Scotia Basin, offshore Atlantic Canada: 1. Comparison of observations with geometrically simple numerical models, *Tectonics*, **29**(TC4017), doi:10.1029/2009TC002539.
- Altenbernd, T., Jokat, W., Heyde, I., & Damm, V., 2014. A crustal model for northern Melville Bay, Baffin Bay, *Journal of Geophysical Research*, **119**(doi:10.1002/2014JB011559), 8610–8632.
- Altenbernd, T., Jokat, W., Heyde, I., & Damm, V., 2015. Geophysical evidence for the extent of crustal types and the type of margin along a profile in the northeastern Baffin Bay, *Journal of Geophysical Research*, **120**(doi:10.1002/2015JB012307), 7337–7360.
- Altenbernd, T., Jokat, W., Heyde, I., & Damm, V., 2016. Insights into the crustal structure of the transition between Nares Strait and Baffin Bay, *Tectonophysics*, **691**(doi:10.1016/j.tecto.2016.04.001), 31–47.
- Alvey, A., Gaina, C., Kuszniir, N., & Torsvik, T., 2008. Integrated crustal thickness mapping and plate reconstructions for the high Arctic, *Earth and Planetary Science Letters*, **274**, 310–321.
- Andersen, O. B., Knudsen, P., & Berry, P. A., 2010. The DNSC08GRA global marine gravity field from double retracked satellite altimetry, *Journal of Geodesy*, **84**(doi: 10.1007/s00190-0355-9), 191–199.
- Athy, L., 1930. Density, porosity, and compaction of sedimentary rocks, *AAPG Bulletin*, **14**(1), 1–24.
- Balkwill, H., McMillan, N., MacLean, B., Williams, G., & Srivastava, S., 1990. Geology of the Labrador Shelf, Baffin Bay, and Davis Strait, in *Geology of the Continental Margin of Eastern Canada*, edited by M. Keen & G. Williams, chap. 7, pp. 295–349, Geological Survey of Canada, Geology of Canada, no.2.

- Balkwill, H. R., 1987. Labrador Basin: structural and stratigraphic style, in *Sedimentary Basins and Basin-Forming Mechanisms*, edited by C. Beaumont & A. Tankard, vol. 12, pp. 17–43, Canadian Society of Petroleum Geologists Memoir.
- Barnett-Moore, N., Müller, D., Williams, S., Skogseid, J., & Seton, M., 2016. A reconstruction of the North Atlantic since the earliest Jurassic, *Basin Research*, (doi:10.1111/bre.12214), 1–26.
- Barrett, D., Keen, C., Manchester, K., & Ross, D., 1971. Baffin Bay: an ocean, *Nature*, **229**, 551–552.
- Boydén, J., Müller, R., Gurnis, M., Torsvik, T., Clark, J., Turner, M., Ivey-Law, H., Watson, R., & Cannon, J., 2011. Next-generation plate-tectonic reconstructions using GPlates, in *Geoinformatics: Cyberinfrastructure for the Solid Earth Science*, edited by G. Keller & C. Baru, pp. 95–114, Cambridge University Press.
- Brune, S., Heine, C., Pérez-Gussinyé, M., & Sobolev, S. V., 2014. Rift migration explains continental margin asymmetry and crustal hyper-extension, *Nature Communications*, **5**:4014 (doi: 10.1038/ncomms5014).
- Cannon, J., Lau, E., & Müller, R., 2014. Plate tectonic raster reconstruction in GPlates, *Solid Earth*, **5**(doi:10.5194/se-5-741-2014), 741–755.
- Chasseriau, P. & Chouteau, M., 2003. 3D gravity inversion using a model of parameter covariance, *Journal of Applied Geophysics*, **52**(1), 59–74.
- Chian, D., Keen, C., Reid, I., & Loudén, K. E., 1995a. Evolution of nonvolcanic rifted margins: new results from the conjugate margins of the Labrador Sea, *Geology*, **23**(7), 589–592.
- Chian, D., Loudén, K. E., & Reid, I., 1995b. Crustal structure of the Labrador Sea conjugate margin and implications for the formation of nonvolcanic continental margins, *Journal of Geophysical Research*, **100**(B12), 24239–24253.
- Cowie, L. & Kusznir, N., 2012. Gravity inversion mapping of crustal thickness and lithosphere thinning for the eastern Mediterranean, *Leading Edge*, **31**(7), 810–814.
- Dahl-Jensen, T., Larsen, T. B., Woelbern, I., Bach, T., Hanka, W., Kind, R., Gergersen, S., Mosegaard, K., Voss, P., & Gudmundsson, O., 2003. Depth to Moho in Greenland: receiver-function analysis suggests two Proterozoic blocks in Greenland, *Earth and Planetary Science Letters*, **205**(3–4), 379–393.
- Darbyshire, F. A., 2003. Crustal structure across the Canadian High Arctic region from teleseismic receiver function analysis, *Geophysical Journal International*, **152**, 372–391.
- Dehler, S. A. & Welford, J. K., 2013. Variations in rifting style and structure of the Scotian margin, Atlantic Canada, from 3D gravity inversion, in *Conjugate Divergent Margins*, edited by W. Mohriak, A. Danforth, P. Post, D. Brown, G. Tari, M. Nemčok, & S. Sinha, vol. 369, pp. 289–300, Geological Society Special Publication.
- Divins, D., 2003. Total sediment thickness of the world's oceans & marginal seas, NOAA National Geophysical Data Center, Boulder, CO.
- Doré, A., Lundin, E., Fichler, C., & Olesen, O., 1997. Patterns of basement structure and reactivation along

- the NE Atlantic margin, *Journal of the Geological Society, London*, **154**(1), 85–92.
- Funck, T., Jackson, H., Loudon, K. E., & ofer, F. K., 2007. Seismic study of the transform-rifted margin in Davis Strait between Baffin Island (Canada) and Greenland: what happens when a plume meets a transform, *Journal of Geophysical Research*, **112**(4), doi:10.1029/2006JB004308.
- Funck, T., Gohl, K., Damm, V., & Heyde, I., 2012. Tectonic evolution of southern Baffin Bay and Davis Strait: results from a seismic refraction transect between Canada and Greenland, *Journal of Geophysical Research*, **117**(4), B04107.
- Geng, M., Welford, J. K., & Farquharson, C. G., 2017. 3D gravity inversion using the constrained stochastic method: applications to crustal-scale models of rifted margins, in *79th EAGE Conference and Exhibition*, Paris, France.
- Geng, M., Welford, J. K., Farquharson, C. G., & Hu, X., submitted. 3-D gravity inversion using the constrained probabilistic method: applications to crustal-scale models of rifted continental margins, *Geophysics*.
- Geoffroy, L., 2001. The structure of volcanic margins: some problematics from the North-Atlantic/Labrador-Baffin system, *Marine and Petroleum Geology*, **18**(doi:10.1016/S0264 8172(00)000738), 463–469.
- Geoffroy, L., Callot, J.-P., Scaillet, S., Skuce, A., Gélard, J., Ravilly, M., Angelier, J., Bonin, B., Cayet, C., Perrot, K., & Lepvrier, C., 2001. Southeast Baffin volcanic margin and the North American Greenland plate separation, *Tectonics*, **20**(4), 566–584.
- Gerlings, J., Funck, T., Jackson, H., Loudon, K. E., & ofer, F. K., 2009. Seismic evidence for plume-derived volcanism during formation of the continental margin in southern Davis Strait and northern Labrador Sea, *Geophysical Journal International*, **176**(3), 980–994.
- Gibbons, A. D., Barckhausen, U., van den Bogaard, P., Hoernle, K., Werner, R., Whittaker, J. M., & Müller, R. D., 2012. Constraining the Jurassic extent of Greater India: tectonic evolution of the West Australian margin, *Geochemistry, Geophysics, Geosystems*, **13**(5), doi:10.1029/2011GC003919.
- Gion, A. M., Williams, S. E., & Müller, R. D., 2017. A reconstruction of the Eureka Orogeny incorporating deformation constraints, *Tectonics*, **36**(doi:10.1002/2015TC004094), 304–320.
- Gregersen, U., Hopper, J. R., & Knutz, P. C., 2013. Basin seismic stratigraphy and aspects of prospectivity in the NE Baffin Bay, Northwest Greenland, *Marine and Petroleum Geology*, **46**, 1–18.
- Grocott, J. & McCaffrey, K. J., 2017. Basin evolution and destruction in an Early Proterozoic continental margin: the Rinkian fold-thrust belt of central West Greenland, *Journal of the Geological Society, London*, **174**(3, <https://doi.org/10.1144/jgs2016-109>).
- Gurnis, M., Yang, T., Cannon, J., Turner, M., Williams, S., Flament, N., & Müller, R., 2018. Global tectonic reconstructions with continuously deforming and evolving rigid plates, *Computers and Geosciences*, **116**(doi:10.1016/j.cageo.2018.04.007), 32–41.

- Heron, P. J., Pysklywec, R. N., & Stephenson, R., 2015. Intraplate orogenesis within accreted and scarred lithosphere: Example of the Eurekan Orogeny, Ellesmere Island, *Tectonophysics*, **664**, 202–213.
- Hosseinpour, M., Müller, R., Williams, S., & Whittaker, J., 2013. Full-fit reconstruction of the Labrador Sea and Baffin Bay, *Solid Earth*, **4**(doi:10.5194/se-4-461-2013), 461–479.
- Huismans, R. & Beaumont, C., 2002. Asymmetric lithospheric extension: the role of frictional plastic strain softening inferred from numerical experiments, *Geology*, **30**, 211–214.
- Jackson, H. & Reid, I., 1994. Crustal thickness variations between Greenland and the Ellesmere Island margin determined from seismic refraction, *Canadian Journal of Earth Sciences*, **31**(9), 1407–1418.
- Jackson, H., Keen, C., & Falconer, R., 1979. New geophysical evidence for sea-floor spreading in central Baffin Bay, *Canadian Journal of Earth Sciences*, **16**, 2122–2135.
- Jackson, H. R., Dickie, K., & Marillier, F., 1992. A seismic reflection study of northern Baffin Bay: implication for tectonic evolution, *Canadian Journal of Earth Sciences*, **29**, 2353–2369.
- Jackson, M. & Talbot, C., 1986. External shapes, strain rates, and dynamics of salt structures, *Bulletin of the Geological Society of America*, **97**(3), 305–323.
- Keen, C. & Barrett, D., 1972. Seismic refraction studies in Baffin Bay: an example of a developing ocean basin, *Geophysical Journal of the Royal Astronomical Society*, **30**, 253–271.
- Keen, C., Barrett, D., Manchester, K., & Ross, D., 1972a. Geophysical studies in Baffin Bay and some tectonic implications, *Canadian Journal of Earth Sciences*, **9**, 239–256.
- Keen, C. E., Dickie, K., & Dehler, S. A., 2012. The volcanic margins of the northern Labrador Sea: insights to the rifting process, *Tectonics*, **31**(TC1011), doi:10.1029/2011TC002985.
- Keen, C. E., Dickie, K., & Dafoe, L. T., 2018. Structural characteristics of the ocean-continent transition along the rifted continental margin, offshore central Labrador, *Marine and Petroleum Geology*, **89**, 443–463.
- Keen, M., Johnson, J., & Park, I., 1972b. Geophysical and geological studies in eastern and northern Baffin Bay and Lancaster Sound, *Canadian Journal of Earth Sciences*, **9**, 689–708.
- Kimbell, G., Ritchie, J., & Henderson, A., 2010. Three-dimensional gravity and magnetic modelling of the Irish sector of the NE Atlantic margin, *Tectonophysics*, **486**, 36–54.
- Larsen, L. M., Heaman, L. M., Creaser, R. A., Duncan, R. A., Frei, R., & Hutchison, M., 2009. Tectono-magmatic events during stretching and basin formation in the Labrador Sea and Davis Strait: evidence from age and composition of mesozoic to palaeogene dykes swarms in West Greenland, *Journal of the Geological Society, London*, **166**, 999–1012.
- Lawver, L., Müller, R., Srivastava, S., & Roest, W., 1990. The opening of the Arctic Ocean, in *Geological history of the polar oceans: Arctic versus Antarctic*, edited by U. Bleil & J. Thiede, vol. 308, NATO ASI Series (Series C: Mathematical and Physical Sciences).
- Li, Y. & Oldenburg, D. W., 1996. 3-D inversion of magnetic data, *Geophysics*, **61**(2), 394–408.

- Li, Y. & Oldenburg, D. W., 1998. 3-D inversion of gravity data, *Geophysics*, **63**, 109–119.
- Louden, K., Tucholke, B., & Oakey, G., 2004. Regional anomalies of sediment thickness, basement depth and isostatic crustal thickness in the North Atlantic Ocean, *Earth and Planetary Science Letters*, **224**(1–2), 193–211.
- Louden, K. E. & Chian, D., 1999. The deep structure of non-volcanic rifted continental margins, *Philosophical transactions of the Royal Society of London*, **357**, 767–804.
- Matthews, K. J., Maloney, K. T., Zahirovic, S., Williams, S. E., Seton, M., & Müller, R. D., 2016. Global plate boundary evolution and kinematics since the late Paleozoic, *Global and Planetary Change*, **146**(doi: 10.1016/j.gloplacha.2016.10.002), 226–250.
- McGregor, E., Nielsen, S., & Stephenson, R., 2014. Basin evolution in the Davis Strait area (West Greenland and conjugate East Baffin/Labrador passive margins) from thermostratigraphic and subsidence modelling of well data: implications for tectonic evolution and petroleum systems, *Bulletin of Canadian Petroleum Geology*, **62**(4), 311–329.
- Müller, D., Russell, S. H., Zahirovic, S., Williams, S. E., & Williams, C. S., 2018. Modelling and visualising distributed crustal deformation of Australia and Zealandia using GPlates 2.0, in *First Australasian Exploration Geoscience Conference (AEGC)*, Sydney, Australia.
- Müller, R., Seton, M., Zahirovic, S., Williams, S., Matthews, K., Wright, N., Shephard, G., Maloney, K., Barnett-Moore, N., Hosseinpour, M., Bower, D., & Cannon, J., 2016. Ocean basin evolution and global-scale plate reorganization events since Pangea breakup, *Annual Reviews of Earth and Planetary Science*, (doi:4410.1146/annurev-earth-060115-012211).
- Nelson, C., Jerram, D., Clayburn, J., Halton, A., & Roberge, J., 2015. Eocene volcanism in offshore southern Baffin Bay, *Marine and Petroleum Geology*, **67**, 678–691.
- Nielsen, S., Stephenson, R., & Thomsen, E., 2007. Dynamics of Mid-Palaeocene North Atlantic rifting linked with European intra-plate deformations, *Nature*, **450**(13), 1071–1074.
- Oakey, G. & Chalmers, J., 2012. A new model for the Paleogene motion of Greenland relative to North America: plate reconstructions of the Davis Strait and Nares Strait regions between Canada and Greenland, *Journal of Geophysical Research, Solid Earth*, **117**(10), doi:10.1029/2011JB008942.
- Oakey, G. & Stark, A., 1995. A digital compilation of depth to basement and sediment thickness for the North Atlantic and adjacent coastal land areas, Open file #3039, 29pp., Geological Survey of Canada.
- Peace, A., 2016. *Structural inheritance and magmatism during continental breakup in West Greenland and Eastern Canada*, Ph.D. thesis, Durham University, 364 p., <http://etheses.dur.ac.uk/11877/>.
- Peace, A., McCaffrey, K., Imber, J., Phethean, J., Nowell, G., Gerdes, K., & Dempsey, E., 2016. An evaluation of Mesozoic rift-related magmatism on the margins of the Labrador Sea: implications for rifting and passive margin asymmetry, *Geosphere*, **12**(6), doi:10.1130/GES01341.1.
- Peace, A., McCaffrey, K., Imber, J., van Hunen, J., Hobbs, R. W., & Wilson, R., in press. The role of pre-

- existing structures during continental breakup and transform system development in the Davis Strait, offshore West Greenland, *Basin Research*, (doi:10.1111/bre.12257).
- Peace, A. L., Foulger, G. R., Schiffer, C., & McCaffrey, K. J., 2017. Evolution of Labrador Sea - Baffin Bay: plate or plume processes?, *Geoscience Canada*, (doi:10.12789/geocanj.2017.44.120).
- Phethean, J., Kalnins, L., van Hunen, J., Biffi, P., Davies, R., & McCaffrey, K., 2016. Madagascar's escape from Africa: a high-resolution plate reconstruction for the Western Somali Basin and implications for supercontinent dispersal, *Geochemistry, Geophysics, Geosystems*, **17**(doi:10.1002/2016GC006406), 2825–2834.
- Reid, I. & Jackson, H., 1997. Crustal structure of northern Baffin Bay: seismic refraction results and tectonic implications, *Journal of Geophysical Research*, **102**(B1), 523–542.
- Riisager, P. & Abrahamsen, N., 1999. Magnetostratigraphy of Paleocene basalts from the Vaigat Formation of West Greenland, *Geophysical Journal International*, **137**, 774–782.
- Sandwell, D. T. & Smith, W. H., 1997. Marine gravity anomaly from Geosat and ERS 1 satellite altimetry, *Journal of Geophysical Research*, **102**(B5), 10039–10054.
- Schiffer, C., Tegner, C., Schaeffer, A. J., Pease, V., & Nielsen, S., 2017. High Arctic geopotential stress field and implications for geodynamic evolution, in *Circum-Arctic Lithosphere Evolution*, edited by V. Pease & B. Coakley, vol. 460, Geological Society London, Special Publications.
- Sclater, J. & Christie, P., 1980. Continental stretching: an explanation of the post-mid-Cretaceous subsidence of the central North Sea Basin, *Journal of Geophysical Research*, **85**(B7), 3711–3739.
- Skaarup, N., Jackson, H., & Oakey, G., 2006. Margin segmentation of Baffin Bay/Davis Strait, eastern Canada based on seismic reflection and potential field data, *Marine and Petroleum Geology*, **23**(1), 127–144.
- Srivastava, S., 1978. Evolution of the Labrador Sea and its bearing on the early evolution of the North Atlantic, *Geophysical Journal of the Royal Astronomical Society*, **52**(2), 313–357.
- St-Onge, M. R., van Gool, J. A., Garde, A. A., & Scott, D. J., 2009. Correlation of Archaean and Palaeoproterozoic units between northeastern Canada and western Greenland: constraining the pre-collisional upper plate accretionary history of the Trans-Hudson orogen, in *Earth Accretionary Systems in Space and Time*, edited by P. Cawood & A. Kröner, vol. 318, pp. 193–235, Geological Society London, Special Publications.
- Stephenson, R., Oakey, G., Schiffer, C., & Jacobsen, B., 2013. Ellesmere Island Lithosphere Experiment (ELLITE): Eureka basin inversion and mountain building, Ellesmere Island, Nunavut, *Geological Survey of Canada Current Research*, **21**(doi:10.4095/292859), 8 p.
- Storey, M., Duncan, R., Pedersen, A., Larsen, L., & Larsen, H., 1998. $^{40}\text{Ar}/^{39}\text{Ar}$ geochronology of the West Greenland Tertiary volcanic province, *Earth and Planetary Science Letters*, **160**, 569–586.
- Suckro, S., Gohl, K., Funck, T., Heyde, I., Ehrhardt, A., Schreckenberger, B., Gerlings, J., Damm, V., &

- Jokat, W., 2012. The crustal structure of southern Baffin Bay: implications from a seismic refraction experiment, *Geophysical Journal International*, **190**(doi:10.1111/j.1365-246X.2012.05477.x), 37–58.
- Suckro, S., Gohl, K., Funck, T., Heyde, I., Schreckenberger, B., Gerlings, J., & Damm, V., 2013. The Davis Strait crust - a transform margin between two oceanic basins, *Geophysical Journal International*, **193**(doi:10.1093/gji/ggs126), 78–97.
- Tarantola, A., 2005. *Inverse problem theory and methods for model parameter estimation*, SIAM: Society for Industrial and Applied Mathematics.
- Tegner, C., Duncan, R., Bernstein, S., Brooks, C., Bird, D., & Storey, M., 1998. ^{40}Ar - ^{39}Ar geochronology of Tertiary mafic intrusions along the East Greenland rifted margin: relation to flood basalts and the Iceland hotspot track, *Earth and Planetary Science Letters*, **156**, 75–88.
- Tegner, C., Storey, M., Holm, P., Thorarinsson, S., Zhao, X., Lo, C.-H., & Knudsen, M., 2011. Magmatism and Eureka deformation in the High Arctic Large Igneous Province: ^{40}Ar - ^{39}Ar age of Kap Washington Group volcanics, North Greenland, *Earth and Planetary Science Letters*, **303**, 203–214.
- Tenzer, R., Hamayun, P., Novák, P., Gladkikh, V., & Vajda, P., 2012. Global crust-mantle density contrast estimated from EGM2008, DTM2008, CRUST2.0, and ICE-5G, *Pure and Applied Geophysics*, **169**, 1663–1678.
- Welford, J. K. & Hall, J., 2007. Crustal structure across the Newfoundland rifted continental margin from constrained 3-D gravity inversion, *Geophysical Journal International*, **171**, 890–908.
- Welford, J. K. & Hall, J., 2013. Lithospheric structure of the Labrador Sea from constrained 3-d gravity inversion, *Geophysical Journal International*, **195**(2), 767–784.
- Welford, J. K., Shannon, P. M., O'Reilly, B. M., & Hall, J., 2010. Lithospheric density variations and Moho structure of the Irish Atlantic continental margin from constrained 3-D gravity inversion, *Geophysical Journal International*, **183**(1), 79–95.
- Welford, J. K., Shannon, P. M., O'Reilly, B. M., & Hall, J., 2012. Comparison of lithosphere structure across the Orphan Basin-Flemish Cap and Irish Atlantic conjugate continental margins from constrained 3D gravity inversions, *Journal of the Geological Society, London*, **169** (4)(doi:10.1144/0016-76492011-114), 405–420.
- Whittaker, R., Hamann, N., & Pulvertaft, T., 1997. A new frontier province offshore northwest Greenland: structure, basin development, and petroleum potential of the Melville Bay area, *AAPG Bulletin*, **81**(6), 978–998.
- Williams, S. E., Müller, R. D., Landgrebe, T. C., & Whittaker, J. M., 2012. An open-source software environment for visualizing and refining plate tectonic reconstructions using high-resolution geological and geophysical data sets, *GSA Today*, **22**(doi:10.1130/GSATG139A.1.), 4–9.
- Wilson, R. W., Klint, K. E. S., van Gool, J. A., McCaffrey, K. J., Holdsworth, R. E., & Chalmers, J. A., 2006. Faults and fractures in central West Greenland: onshore expression of continental break-up and

sea-floor spreading in the Labrador-Baffin Bay Sea, *Geological Survey of Denmark and Greenland Bulletin*, **11**, 185–204.

FIGURE CAPTIONS

Fig. 1. Regional bathymetric map of Baffin Bay from the 2014 global 30-arcsec gridded bathymetric data set (http://www.gebco.net/data_and_products/gridded_bathymetry_data) of the General Bathymetric Chart of the Oceans (GEBCO). The red box outlines the region used for the constrained 3-D gravity inversion using GRAV3D. The smaller dashed black box outlines the region used for the constrained 3-D probabilistic gravity inversion. Abbreviations: EI, Ellesmere Island; FB, Foxe Basin; LS, Lancaster Sound; MB, Meville Bay; NS, Nares Strait.

Fig. 2. Bathymetric map of study area (gray shaded) overlain by offshore geological interpretation of volcanics, oceanic crust, and transitional crust, adapted from Oakey and Chalmers (2012), Hosseinpour et al. (2013), and Altenbernd et al. (2015; 2016). Contour interval is 500 m. Onshore, the transition from Archean cratons in the north to Proterozoic orogens in the south is marked by question marks and follows Darbyshire (2003) for Baffin Island and St-Onge et al. (2009) for Greenland. The locations of onshore broad-band seismic stations from Darbyshire (2003) and Dahl-Jensen et al. (2003) are plotted as purple and pink triangles, respectively. This map, and all subsequent maps with eastings and northings, are plotted using UTM zone 19N and the WGS-84 Ellipsoid. Abbreviations: COB, continent-ocean boundary; DB, Disko Bay; EI, Ellesmere Island; LS, Lancaster Sound; MB, Meville Bay; NS, Nares Strait; UFZ, Ungava Fault Zone.

Fig. 3. Comparison between A) the observed free air gravity data over the study area and B) the predicted data generated from the density anomaly model obtained from the constrained 3-D gravity inversion using GRAV3D. The difference between the two datasets is plotted in panel C. Crustal-scale refraction lines are plotted on all three maps for reference (A14, Altenbernd et al. (2014); A15, Altenbernd et al. (2015); A16, Altenbernd et al. (2016); F12, Funck et al. (2012); R1, R2, R3, and R4, Jackson & Reid (1994) and Reid & Jackson (1997); S12, Suckro et al. (2012); S13, Suckro et al. (2013)). Onshore, the transition from Archean cratons in the north to Proterozoic orogens in the south is marked by the dashed gray lines overlain by question marks and follows Darbyshire (2003) for Baffin Island and St-Onge et al. (2009) for Greenland. Abbreviations: DB,

Disko Bay; EI, Ellesmere Island; FB, Foxe Basin; LS, Lancaster Sound; MB, Meville Bay; NS, Nares Strait.

Fig. 4. A) Bathymetry (500 m contour interval) and B) depth to basement (1000 m contour interval) constraints used for the regional 3-D gravity inversions. The dashed blue line on each map shows the continent-ocean boundary from Hosseinpour et al. (2013). The depth to basement map was obtained by interpolating between depth-converted basement picks along proprietary seismic reflection lines on the Canadian margin (extent outlined by thick dotted black line), minimum sediment thickness constraints from NOAA (extent of constraints outlined by dashed purple line), and depth to basement constraints from seismic refraction modelling where no other constraints were available. The anomalously deep basin at the end of line R4 is only constrained by that refraction line but does not adversely influence the inversion as the deep sediments have densities similar to crystalline crust. Onshore, the transition from Archean cratons in the north to Proterozoic orogens in the south is marked by the dashed gray lines overlain by question marks and follows Darbyshire (2003) for Baffin Island and St-Onge et al. (2009) for Greenland. Abbreviations: COB, continent-ocean boundary; DB, Disko Bay; EI, Ellesmere Island; FB, Foxe Basin; LS, Lancaster Sound; MB, Meville Bay; NS, Nares Strait.

Fig. 5. (A) Plot of density versus depth for pure sandstone, for pure shale, for a sandstone and shale mix, and for the average curve for the Nova Scotian margin. (B) Plot of assigned depth-dependent starting densities (thick black constant density lines) and allowable range of densities (grey areas) for sediments in the inversion. For (A), all curves were computed using Athy's law (Athy, 1930) with the sandstone and shale constraints obtained using average trends in passive margin basins from the Gulf of Mexico (Jackson & Talbot, 1986) and the North Sea (Sclater & Christie, 1980). The average curve for the Scotian margin was compiled by Albertz et al. (2010). For (B), the curves from (A) are replotted in white for reference.

Fig. 6. Maps of the depth to the proxy Moho from the inverted 3-D density model using GRAV3D

(A) and the seismic Moho from the smoothly interpolated crustal seismic refraction lines in Baffin Bay and teleseismic studies around Baffin Bay (C). These regional Moho estimates are each combined with the depth to basement constraints (Fig. 3) to derive two estimates of crustal thickness, one from the gravity inversion (B) and the other from the interpolated seismic Moho (D). All maps are plotted with a contour interval of 2 km. Crustal-scale refraction lines are plotted on all maps for reference. The locations of onshore broad-band seismic stations from Darbyshire (2003) and Dahl-Jensen et al. (2003) are plotted as purple and pink triangles, respectively, along with the crustal thicknesses derived from those studies. Onshore, the transition from Archean cratons in the north to Proterozoic orogens in the south is marked by the dashed gray lines overlain by question marks and follows Darbyshire (2003) for Baffin Island and St-Onge et al. (2009) for Greenland. Abbreviations: DB, Disko Bay; EI, Ellesmere Island; FB, Foxe Basin; LS, Lancaster Sound; MB, Meville Bay; NS, Nares Strait.

Fig. 7. Slices through the inverted 3-D density anomaly model from GRAV3D along labeled seismic refraction lines shown on the crustal thickness map (top right, reproduced from Fig. 6). A comparison between the observed free air gravity anomalies (thick black line) and the anomalies predicted for the inverted density anomaly model (red line) is plotted above each slice. The overlain thick black lines on the density anomaly slices correspond to the Moho depths obtained from the seismic refraction studies and the dashed black lines correspond to the Moho proxy depths derived from the gravity inversion. Abbreviations: DB, Disko Bay; EI, Ellesmere Island; FB, Foxe Basin; LS, Lancaster Sound; MB, Meville Bay; NS, Nares Strait.

Fig. 8. Slices through the inverted 3-D density anomaly model from GRAV3D obtained when the interpolated seismic Moho (Fig. 6C) is explicitly used to define a crustal layer in the inversion. The seismic refraction lines along which the slices were extracted are shown on the crustal thickness map derived using the interpolated seismic Moho and the depth to basement constraints (top right, reproduced from Fig. 6D). A comparison between the observed free air gravity anomalies (thick black line) and the anomalies predicted for the inverted density anomaly model (red line) is

plotted above each slice. The overlain thick black lines on the density anomaly slices correspond to the Moho depths obtained along each specific refraction line and these may conflict with the interpolated seismic Moho where coincident refraction lines showed differing Moho depths. The dashed black lines correspond to the Moho proxy depths used to define the Moho in the inversion without the seismic Moho explicitly included as a constraint (Fig. 6). Abbreviations: DB, Disko Bay; EI, Ellesmere Island; FB, Foxe Basin; LS, Lancaster Sound; MB, Meville Bay; NS, Nares Strait.

Fig. 9. Comparison between select slices through the inverted models from A) the GRAV3D inversion without Moho constraints, B) the GRAV3D inversion with a forced Moho boundary, and C) the probabilistic inversion using sparse Moho constraints. A comparison between the observed free air gravity anomalies (thick black line) and the anomalies predicted for the inverted density anomaly model (red line) is plotted above each slice. The overlain thick black lines on the density anomaly slices correspond to the Moho depths obtained along each specific refraction line. The dashed black lines correspond to 70 kg/m^3 (corresponding to an absolute density of 3020 kg/m^3), the density anomaly chosen as the Moho proxy depth.

Fig. 10. Arbitrary slices through the inverted models from the GRAV3D inversion without Moho constraints (left), and the probabilistic inversion using sparse Moho constraints (right). The slice locations are shown A) on the crustal thickness map derived from the GRAV3D inversion without Moho constraints, B) on the crustal thickness map derived from the probabilistic inversion with sparse Moho constraints, and C) on the crustal thickness difference map between the two methods. On each slice, the dashed black lines correspond to 70 kg/m^3 (corresponding to an absolute density of 3020 kg/m^3), the density anomaly chosen as the base of the crust/Moho proxy depth. The thinner dashed blue line on each slice corresponds to the base of the crust/Moho proxy along the co-located slice from the other inversion method for direct comparison. Abbreviations: DB, Disko Bay; EI, Ellesmere Island; FB, Foxe Basin; LS, Lancaster Sound; MB, Meville Bay; NS, Nares Strait.

Strait.

Fig. 11. Comparison between the crustal thicknesses from the gravity inversion from GRAV3D (A) and the interpolated seismic Moho (B) against crustal thickness estimates computed using GPlates for different initial crustal thicknesses (34, 36, 38, and 40 km) and deformation zone half-widths (150, 300, and 450 km). The results from the GPlates modelling have been cropped to match the model extent from the gravity inversion. Contour interval for all maps is 2 km. Abbreviations: COB, continent-ocean boundary; DB, Disko Bay; EI, Ellesmere Island; LS, Lancaster Sound; MB, Meville Bay; NS, Nares Strait.

Fig. 12. Crustal thickness for a 300 km wide half-width rift zone and an initial, pre-rift, uniform crustal thickness of 34 km after 20, 55, 60, 65, 80, and 120 Ma years of deformation. Baffin Island remains fixed in all of the plots. COBs are shown in blue (Hosseinpour et al., 2013) whilst the limits of the deformable zone are shown in purple (see Gion et al. (2017) for the northern boundary). Contour interval for all maps is 2 km. The colourbar is identical to that of Figure 11, allowing for a direct comparison of crustal thicknesses to be made.

Fig. 13. Comparison between A) the bathymetry overlain by the geological interpretation from Fig. 2, B) the derived crustal thickness map from the GRAV3D gravity inversion without Moho constraints (contour interval of 2 km), and C) the difference between the map in (B) and the crustal thicknesses derived from the probabilistic inversion (Fig. 10C). The Eocene spreading centres are overlain on the crustal thickness map as dashed gray lines where they appear to coincide with the thinnest crust. The thick orange lines on the crustal thickness map correspond to regions where higher density lower crust is required to reproduce the observed gravity data when the seismic Moho is included as a continuous boundary layer constraint in the GRAV3D inversion. Onshore, the transition from Archean cratons in the north to Proterozoic orogens in the south is marked by the dashed gray lines overlain by question marks and follows Darbyshire (2003) for Baffin Island and St-Onge et al. (2009) for Greenland. Abbreviations: COB, continent-ocean boundary; DB,

Disko Bay; EI, Ellesmere Island; LS, Lancaster Sound; MB, Meville Bay; NS, Nares Strait; UFZ, Ungava Fault Zone.

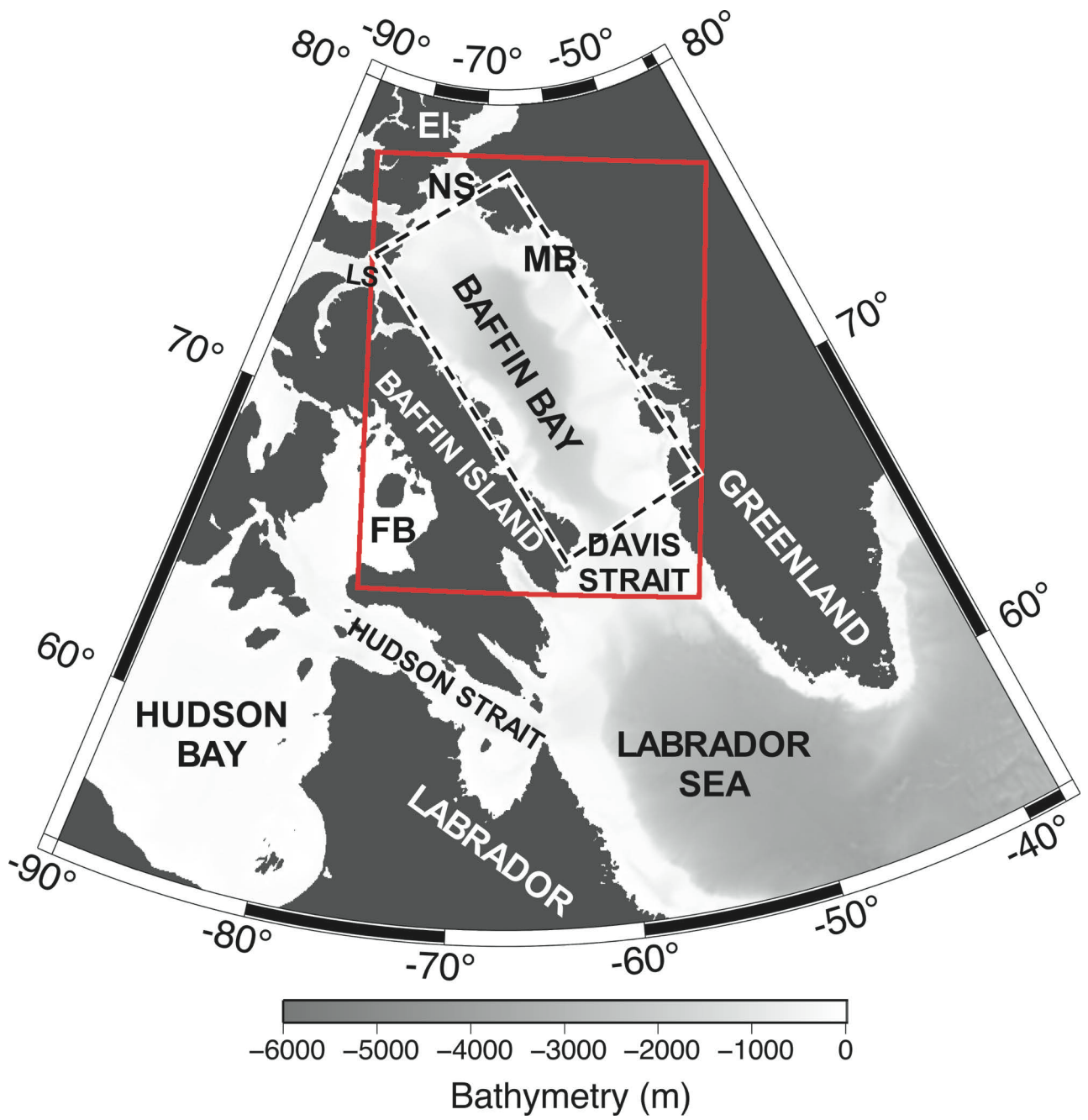


Figure 1.

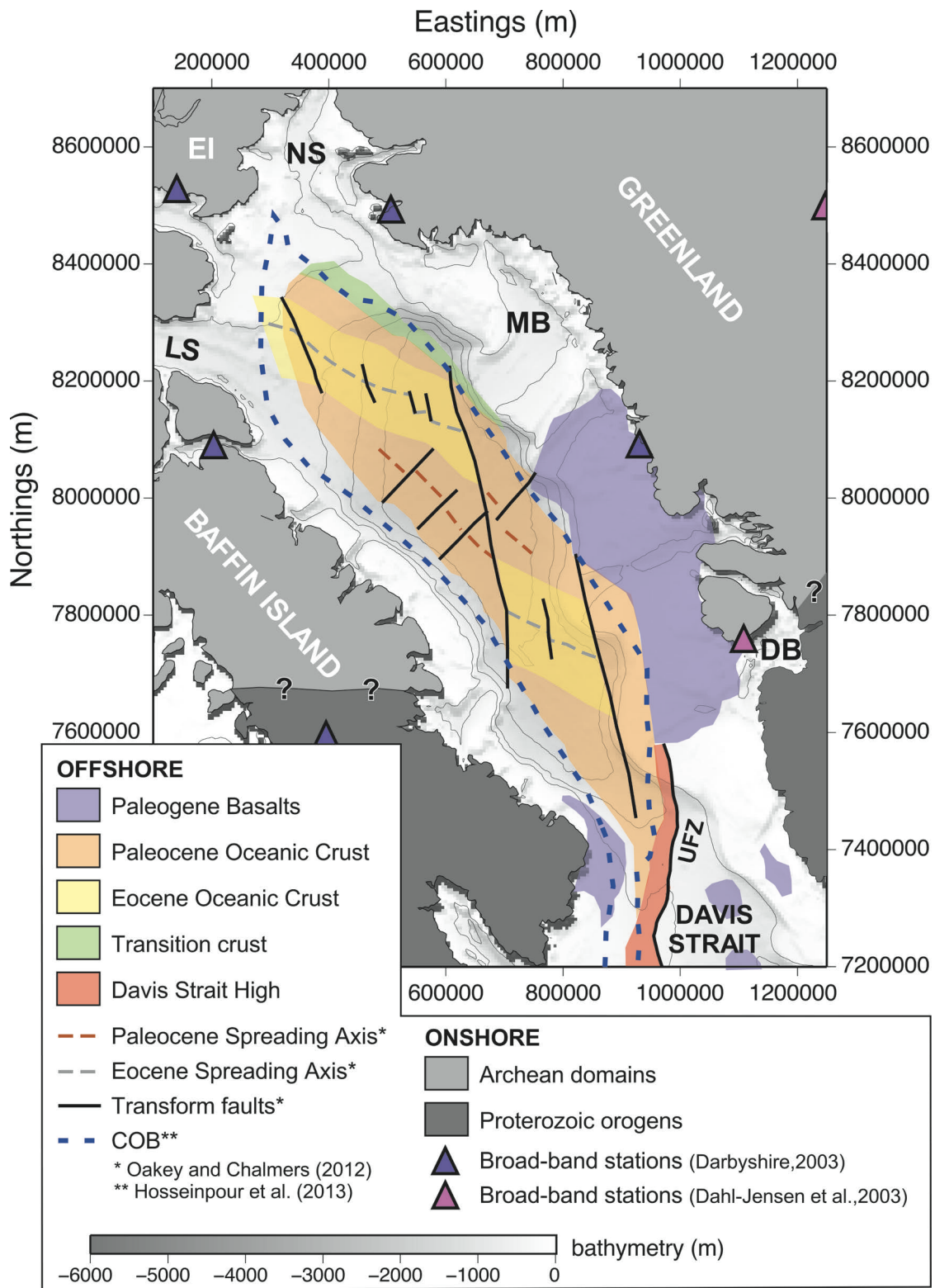


Figure 2.

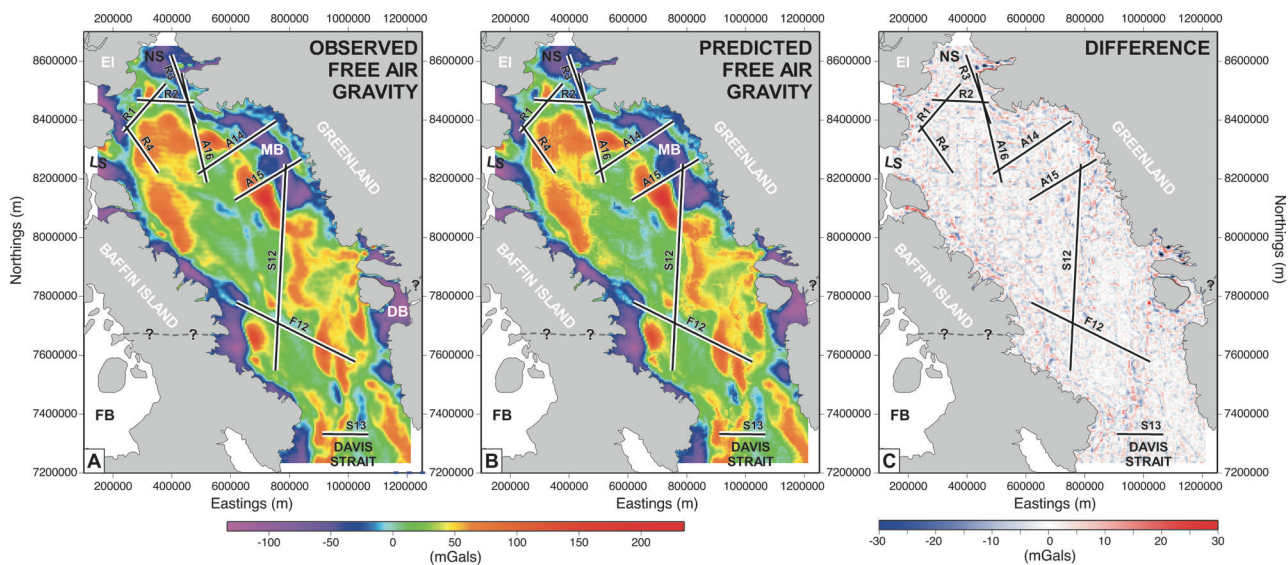


Figure 3.

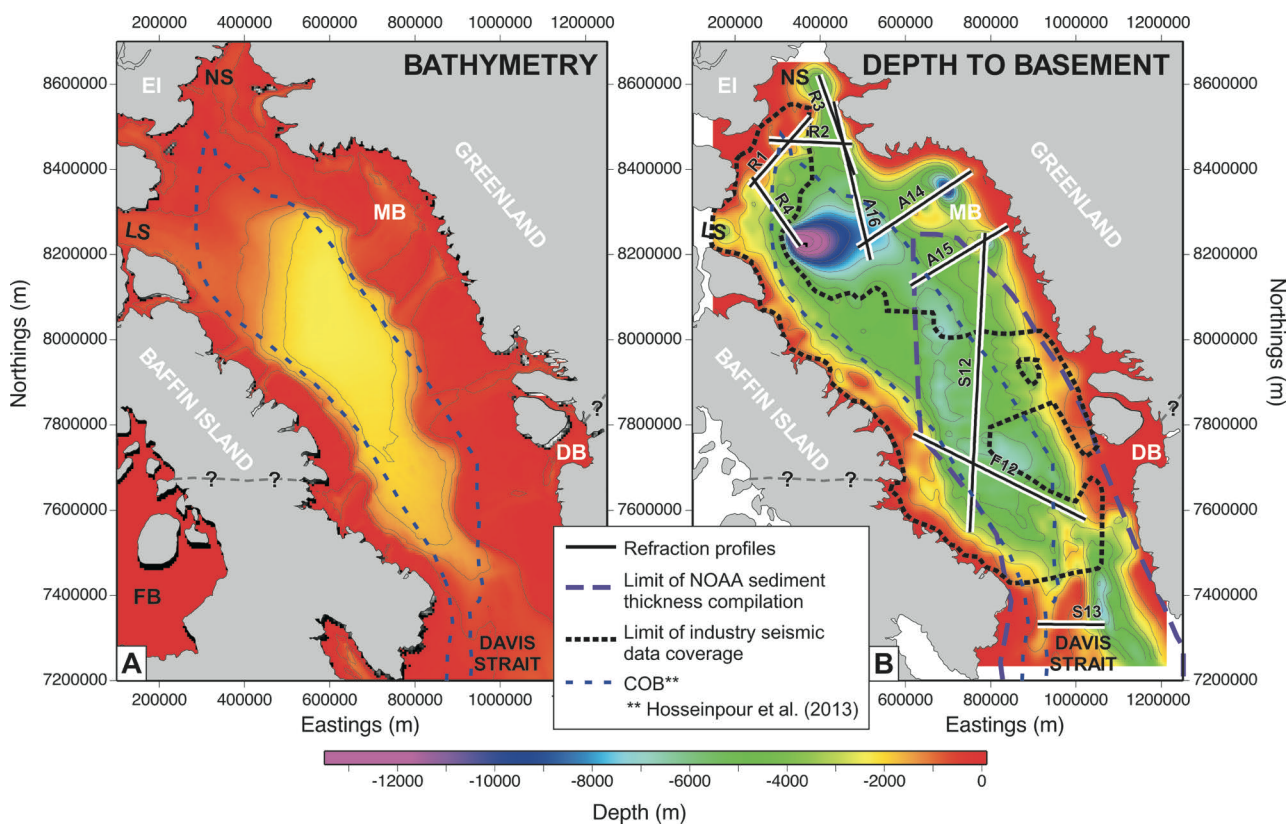


Figure 4.

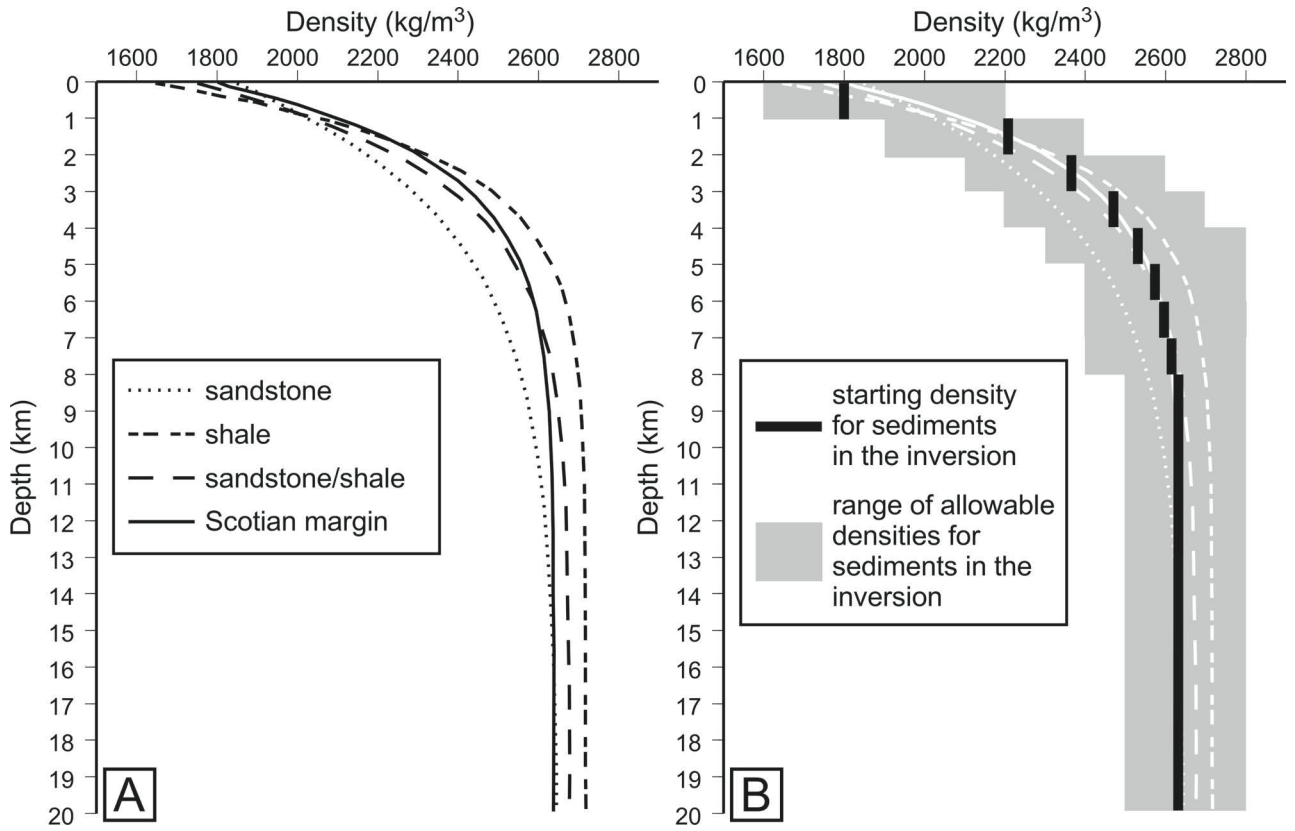


Figure 5.

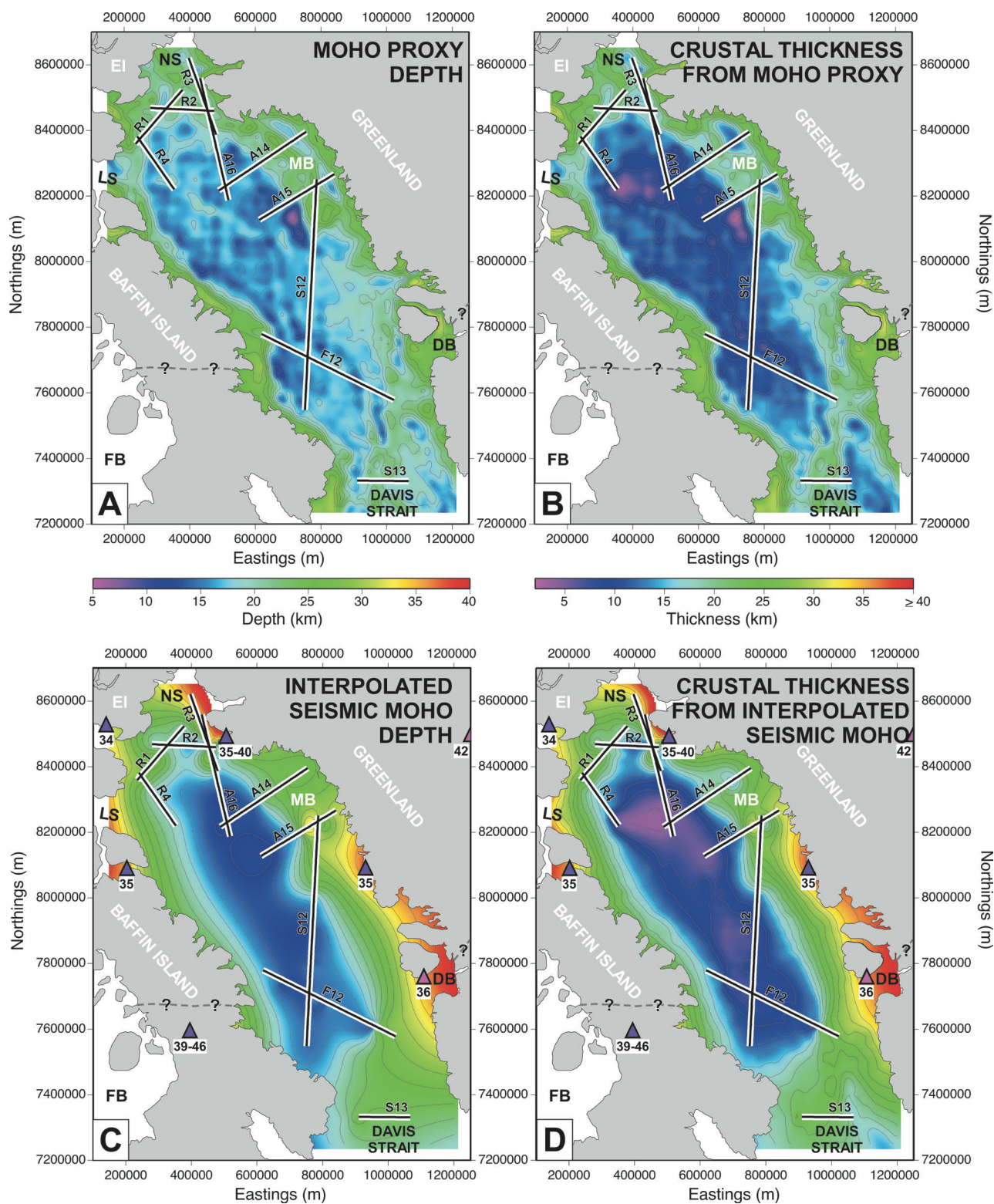


Figure 6.

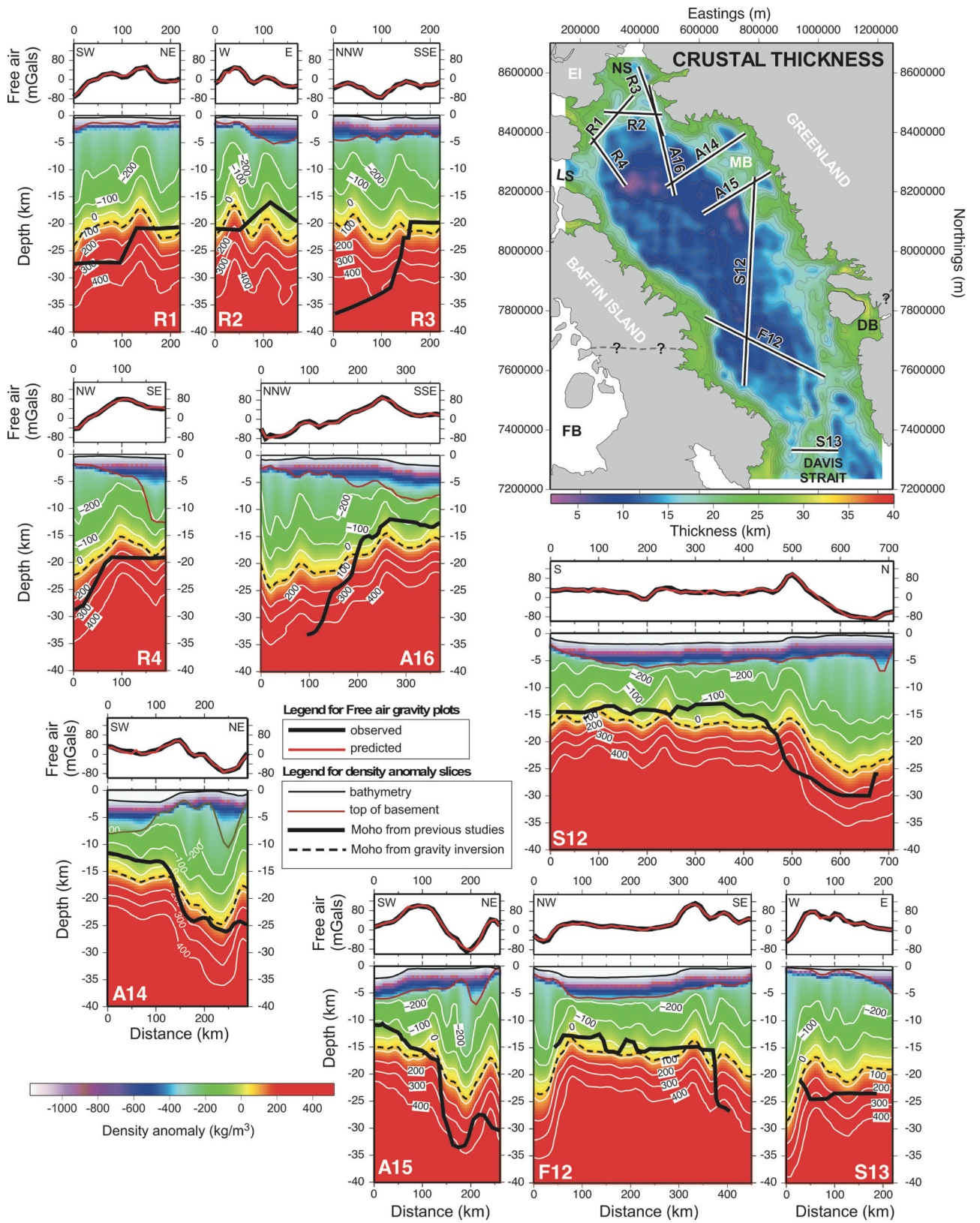


Figure 7.

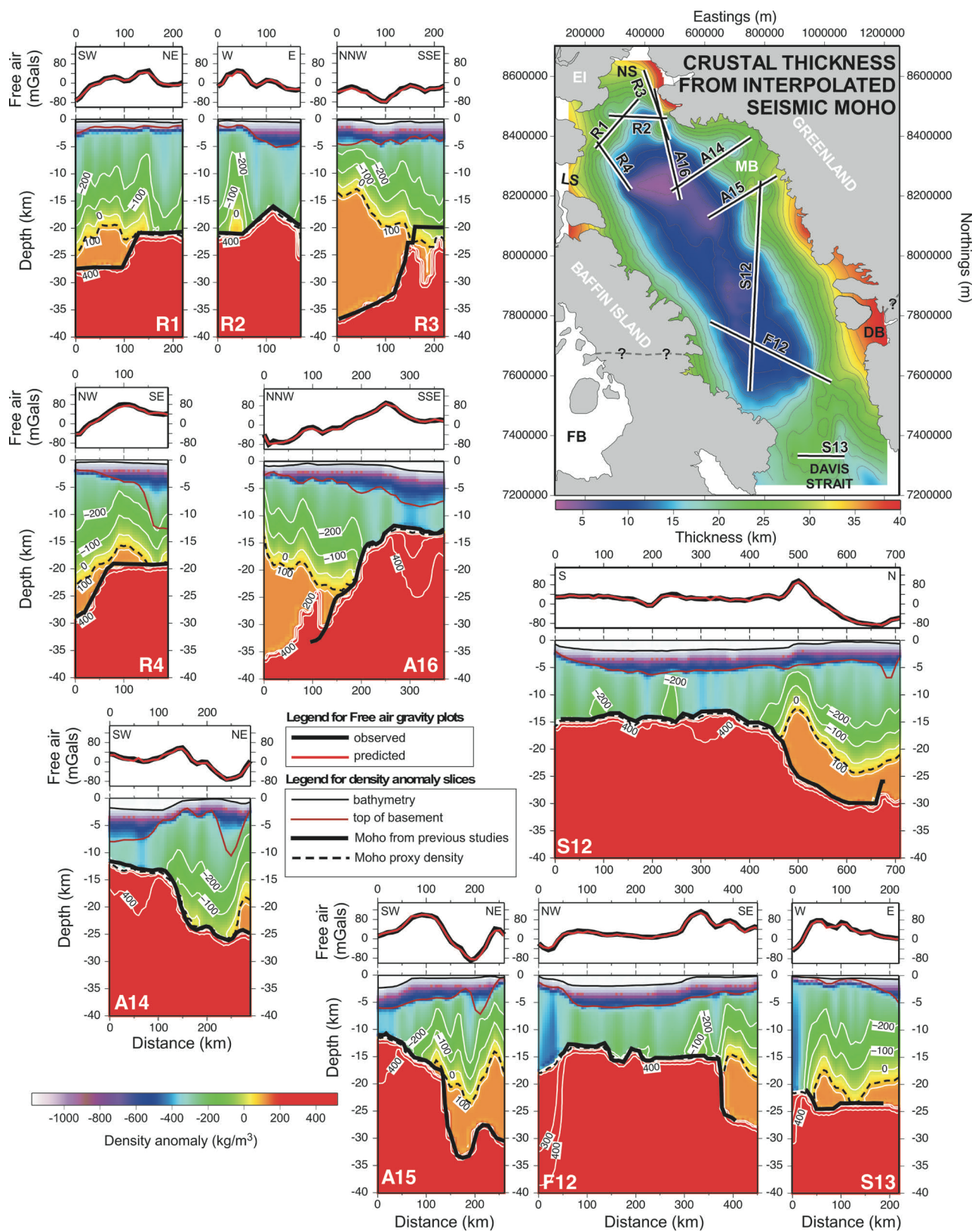


Figure 8.

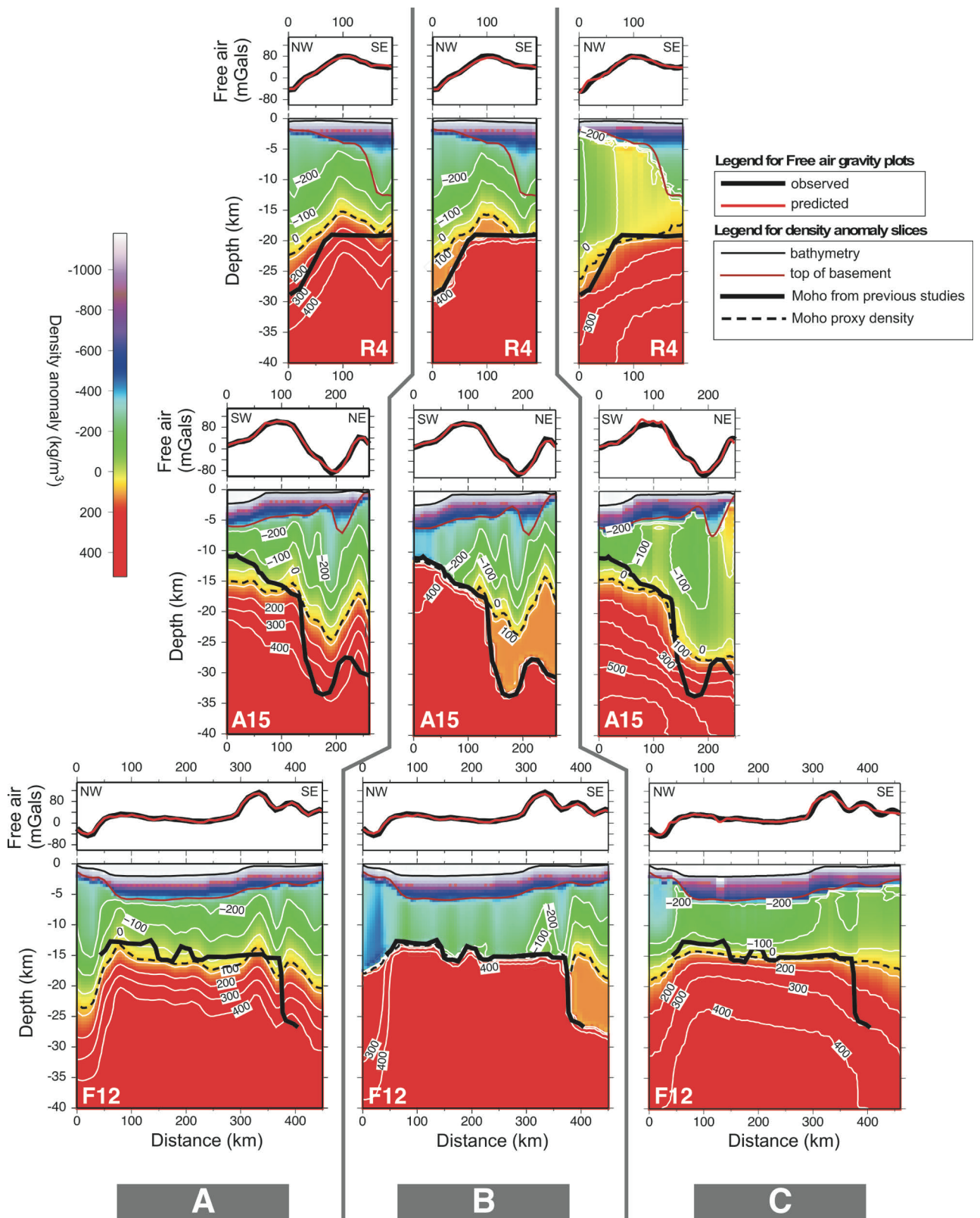


Figure 9.

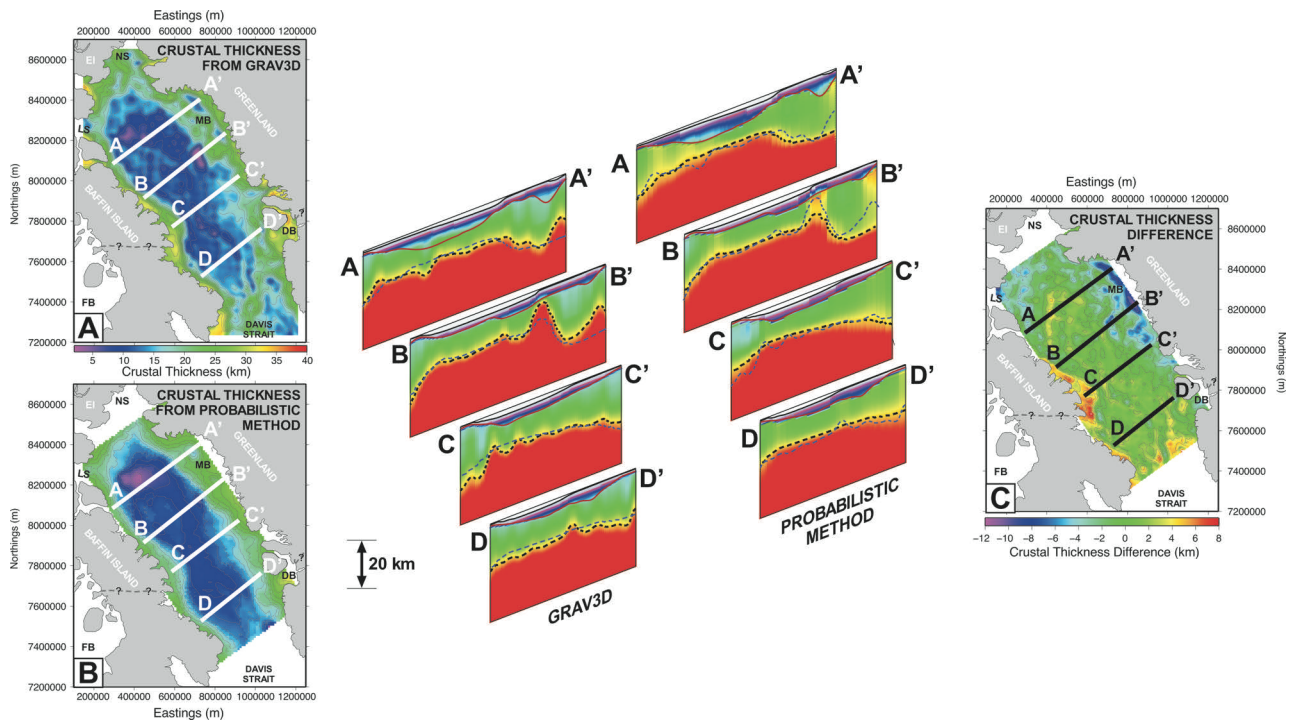


Figure 10.

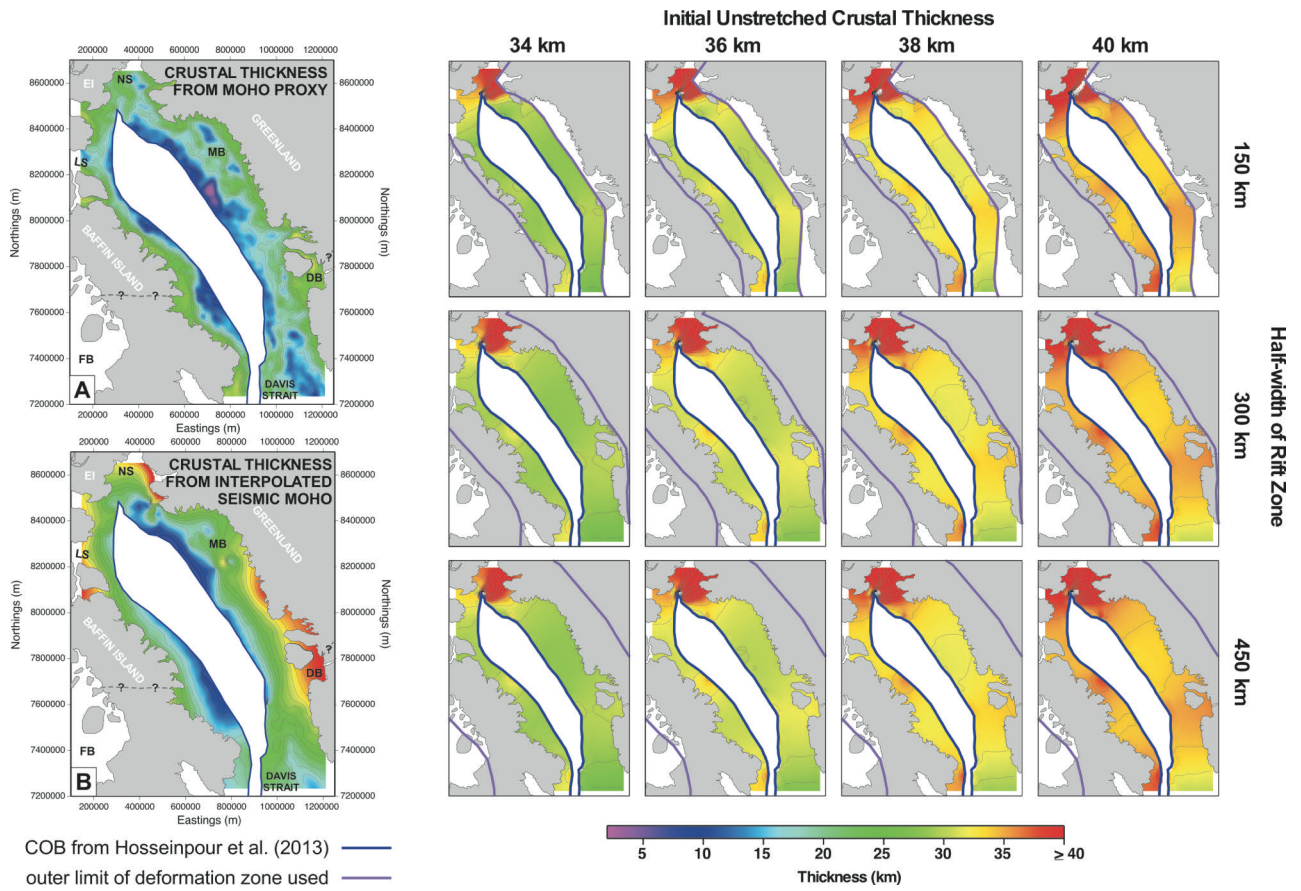


Figure 11.

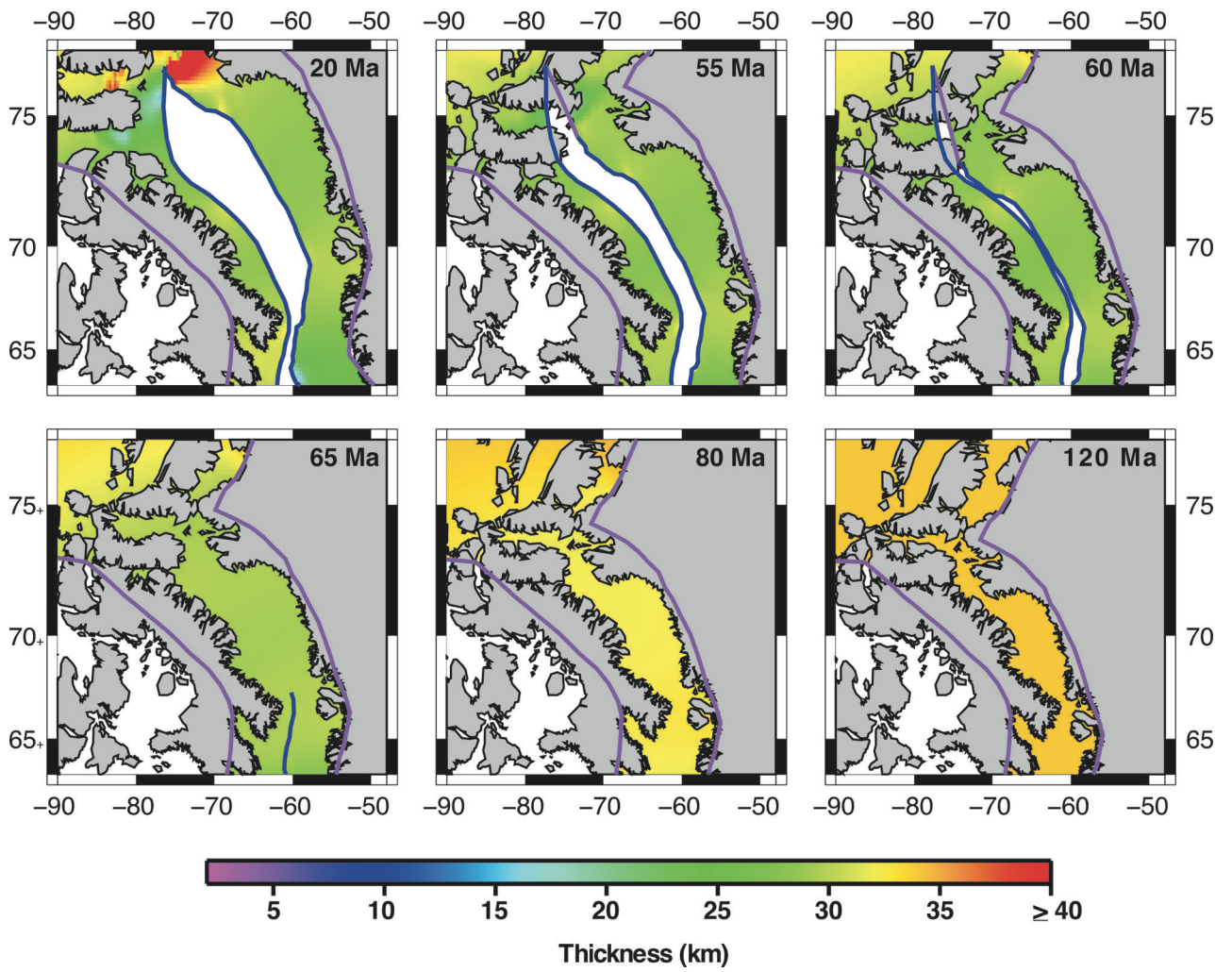


Figure 12.

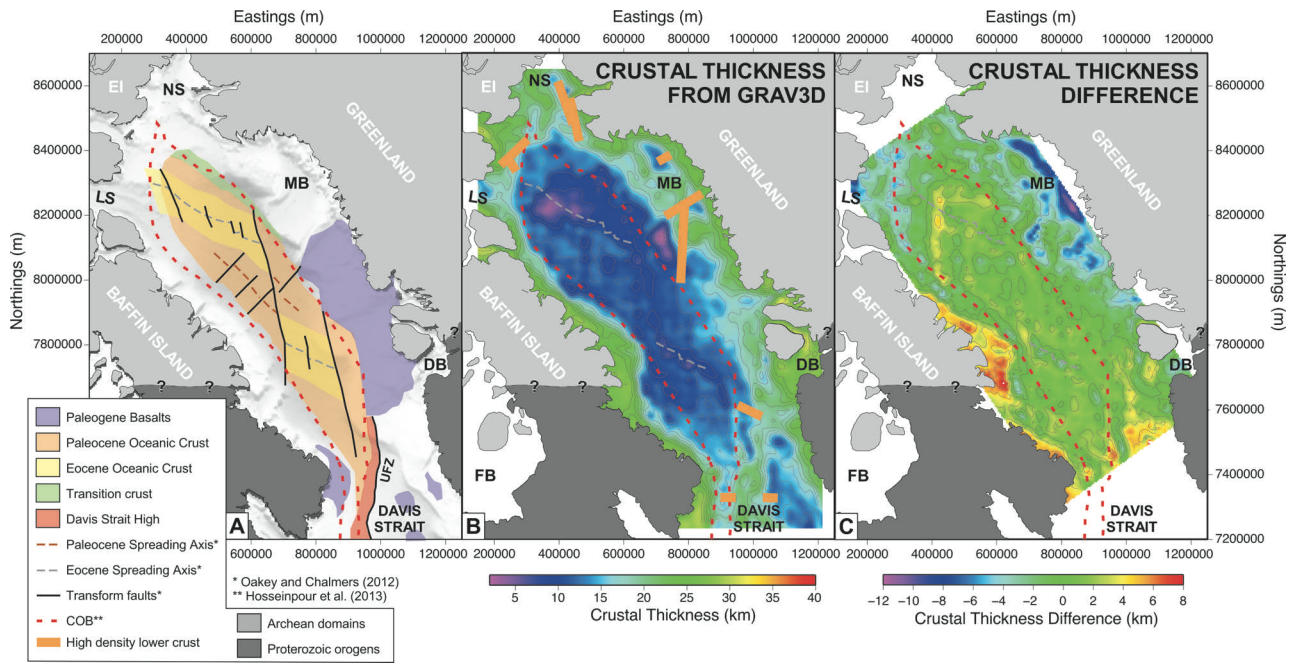


Figure 13.